Received: 7 May 2020 | Revised: 18 July 2020 | Accepted: 21 July 2020

DOI: 10.1002/gj.3959



WILEY

RESEARCH ARTICLE

# Gold, uranium, thorium, and rare earth mineralization in the Kadiri Volcanic Province of Eastern Dharwar Craton, India: An evaluation of mineralogical, textural, and geochemical attributes

Chakravadhanula Manikyamba[1] | Naresh C Ghose[2] | Sohini Ganguly[3] | Arijit Pahari[1] | Challa Satyasri Sindhuja[1]

[1]Geochemistry Division, CSIR-National Geophysical Research Institute, Hyderabad, India

[2]Patna University, Patna, India

[3]School of Earth, Ocean and Atmospheric Sciences, Goa University, Taleigao Plateau, Goa, India

**Correspondence**
Chakravadhanula Manikyamba, CSIR-National Geophysical Research Institute, Uppal Road, Hyderabad 500007, India.
Email: cmaningri@gmail.com

**Funding information**
Council of Scientific and Industrial Research, Grant/Award Number: MLP 6406-28 (CM); Department of Science and Technology, India, Grant/Award Number: ST SR/S4/ES-510/2010; DST Inspire Faculty Project, Grant/Award Number: IFA14-EAS-25

**Handling Editor:** L. Tang

In this article, we present the textural, mineralogical, and geochemical studies of a suite of volcanic rocks and their economic mineral potential from the Kadiri Volcanic Province (KVP) – a greenstone belt in the Eastern Dharwar Craton (EDC) of southern peninsular India. The volcanic rocks are represented by primary pyroclastic deposits dominated by tuff breccia, minor lapilli tuff, and pyroclastic flows together with lava flows, namely, metabasalts, andesites, dacites, and rhyolites. Metabasalts and high-Mg andesites in the KVP are associated with sporadic occurrences of disseminated-type gold. The ancient works on gold are confined to the ductile-brittle shear zones in en-echelon pattern. The source of gold is likely to be from deep fractures (>200 km) at mantle depths that paved the magma to move upper crustal levels due to partial melting of peridotites which tapped the siderophile elements (Au–Ag) from deeper source. Some andesites and dacites contain atomic minerals [uranium, thorium, and rare earth element (REE)], which requires attention in future studies. Monazite occurring in such dacites is a major source of REE such as cerium (Ce), lanthanum (La), neodymium (Nd), and Yttrium (Y), contributing 50–60% of REEs. Presence of thorite ($ThSiO_4$) in dacite, a metamict mineral, strongly radioactive containing upto 10% uranium (U). This study confirms multi-metal mineralization in KVP, for example, gold, silver, atomic (U and Th), rare-earths along with base metals.

Emplacements of rhyolite and alkali granite appears to be synchronous with the major thermal event at 2.51 Ga of the Dharwar Craton. The diverse volcanic associations are formed in a subduction–accretion orogeny at ~2.7 Ga, coeval with the global accretion event and gold mineralization. Au–U–Th–REE abundances in the composite arc-back arc system of Kolar-Hutti-Kadiri-Jonnagiri greenstone belts of EDC are primarily attributed to devolatilization and melting of subducted oceanic slab, fluid-fluxed metasomatism of mantle wedge and elemental cycling associated with different stages of subduction.

**KEYWORDS**
Eastern Dharwar Craton, gold, Kadiri Volcanic Province, Neoarchean, rare earth mineral

  

## 1 | INTRODUCTION

Continental growth is an ever-changing process closely linked with the condensation of the Earth and magmatism/volcanism. Since the Hadean (4.5 Ga), the development of crust, its merger or break-up by collision and amalgamation are fashioned since the birth of the Earth (Hawkesworth & Kemp, 2006; Roberts, 2012; Santosh, 2010; Santosh, Arai, & Maruyama, 2017). Advances in science made it plausible to a better understanding on the distribution of land and sea and the processes operating in changing the face of the Earth. Application of geochemistry and isotopic studies has contributed a fair degree of accuracy to understand the tectonic setting of rocks. Studies on the Phanerozoic tectono-magmatic processes provide significant information to evaluate and correlate the processes involved in the development of ancient crust.

The phenomenon of mineral endowment of Archean greenstone belts hinges upon a conjunction of magmatic, sedimentary, and metamorphic processes that operated in different geodynamic settings and collectively contributed towards the nature and diversity of mineralization (Ganguly & Yang, 2018; Manikyamba, Ganguly, Santosh, & Subramanyam, 2017). However, the processes involved in the genesis of some rock types such as volcanic agglomerates and their mineral potential is an enigma. It is emphasized that the magma generated at depth carries the entire history engraved in it until its expulsion through a vent on the surface of crust as ash particulate (Ghose, 2019). The spatial and temporal distribution of metallogenic associations in Archean granite-greenstone terranes is marked by a heterogeneity as recorded by (a) Pb and sulfate-rich volcanogenic massive sulphides (VMS), porphyry style Mo–Cu and evaporative baryte deposits of 3.5–3.3 and 3.0–2.7 Ga greenstone sequences conforming to shallow marine to subaerial environments and (b) komatiite-associated Ni–Cu deposits, VMS, base metal, and gold mineralization associated with greenstones formed in deeper basins. Iron and manganese mineralization have been attributed to hydrothermal processes associated with midoceanic ridge-rift system. In contrast, gold, Cu porphyry, and VMS Cu–Zn deposits show prominent affinity towards metallogenic processes operative in Archean subduction environments. Hence, diverse geodynamic conditions including mantle plume activity, divergent and convergent margin processes substantiate the heterogeneous mineral endowment of Archean greenstone belts (Ganguly & Yang, 2018; Manikyamba, Ganguly, et al., 2014; Manikyamba, Saha, et al., 2014).

Mineralogy is a key parameter in determining the ease or difficulty, and therefore in turn, the cost of processing and extraction of rare earth elements (REE). Primary, hard rock deposits with the most abundant REE minerals such as bastnäsite, monazite, xenotime, loparite, parasite, and perhaps apatite are more likely to be economically potential with respect to those deposits with eudialyte, allanite, or zircon (Chakhmouradian & Wall, 2012). The latter group is more refractory and economic processing of REE from these minerals is not currently possible. It has been advocated that 30–90% of the REE in the deposit occur (a) as cations in exchangeable sites on clay minerals such as halloysite, kaolinite, and on iron and manganese oxides, (b) as colloids, (c) in secondary phosphate minerals, most commonly monazite and apatite (or florenceite) (d) as secondary oxides, such as cerianite ($CeO_2$), containing REE and (e) as residual REE-bearing minerals, including monazite and xenotime. The distribution and mobility of REE serve as important geochemical tracers of earth science processes including crustal evolution, magma genesis and differentiation, metamorphism, groundwater and soil dynamics and estimation for residence time of particles in the seawater column (Berger et al., 2014). REEs are also of economic interest because of their increasing use in high-tech industries (Chakhmouradian & Wall, 2012). REE concentrations and fractionation depend on the bedrock composition, the physicochemical conditions and the alteration fluid (pH, Eh, ligands in solution, water rock ratio (Price, Maillet, McDougall, & Dupont, 1991), the secondary mineralogy (Banfield & Eggleton, 1989) and the microbial activity (Taunton, Welch, & Banfield, 2000). In felsic rocks, REEs are mainly bound in phosphates (monazite, xenotime, and apatite) or the silicate allanite (Bea, 1996). These accessory phases may break down during weathering (Braun, Pagel, Herbilln, & Rosin, 1993; Price, Velbel, & Patino, 2005). Alteration of the accessory minerals has been studied experimentally using dissolution experiments (Oelkers & Poitrasson, 2002) or through petrological studies of natural samples (Braun et al., 1993; Poitrasson, 2002; Price et al., 2005).

Present study is aimed to examine the textures and mineralogy of the volcanic agglomerates and associated metavolcanic rocks from Kadiri greenstone belt of Eastern Dharwar Craton which provide significant information in understanding the formation of Late Archean crust and associated economic mineral resources besides unravelling the past history.

## 2 | GEOLOGICAL SETTING

The Dharwar Craton (DC) of southern peninsular India is one of the largest cratons ($4.5 \times 10^5$ km$^2$) in Indian subcontinent (Figure 1) with crystalline basement ranging in age from Palaeoarchean to the Early Palaeoproterozoic (Balakrishnan, Rajamani, & Hanson, 1999; Chadwick, Vasudev, & Hegde, 2000; Naqvi, 2005; Nasheeth, Okudaira, Horie, Hokada, & Satish-Kumar, 2015; Peucat, Mahabaleshwar, & Jayananda, 1993; Ramakrishnan & Vaidyanadhan, 2008). The abundance of greenstone belts, basement gneisses, metamorphism, and crustal thickness have categorized the DC into two distinctive sectors, namely, the Western (WDC) and the Eastern Dharwar Craton (EDC; Figure 1; Table 1; Chardon, Jayananda, Chetty, & Peucat, 2008; Gupta et al., 2003; Jayananda, Chardon, Peucat, & Capdevila, 2006; Swami Nath, Ramakrishnan, & Viswanatha, 1976) which are separated by N-S trending Chitradurga shear zone. The WDC is predominantly composed of greenstones and Tonalite-Trondjhemite-Granodiorite (TTG), which show polyphase deformation (Mukhopadhyay, 1986; Naha, Mukhopadhyay, Dastidar, & Mukhopadhyay, 1995) in which two generations of greenstone sequences are recognized. The older Sargur Group (>3.2 Ga) and the younger Dharwar Supergroup (2.9–2.5 Ga; Hokada et al., 2013; Pahari et al., 2019). The Dharwar Group consisting of Bababudan and Chitradurga groups in which the

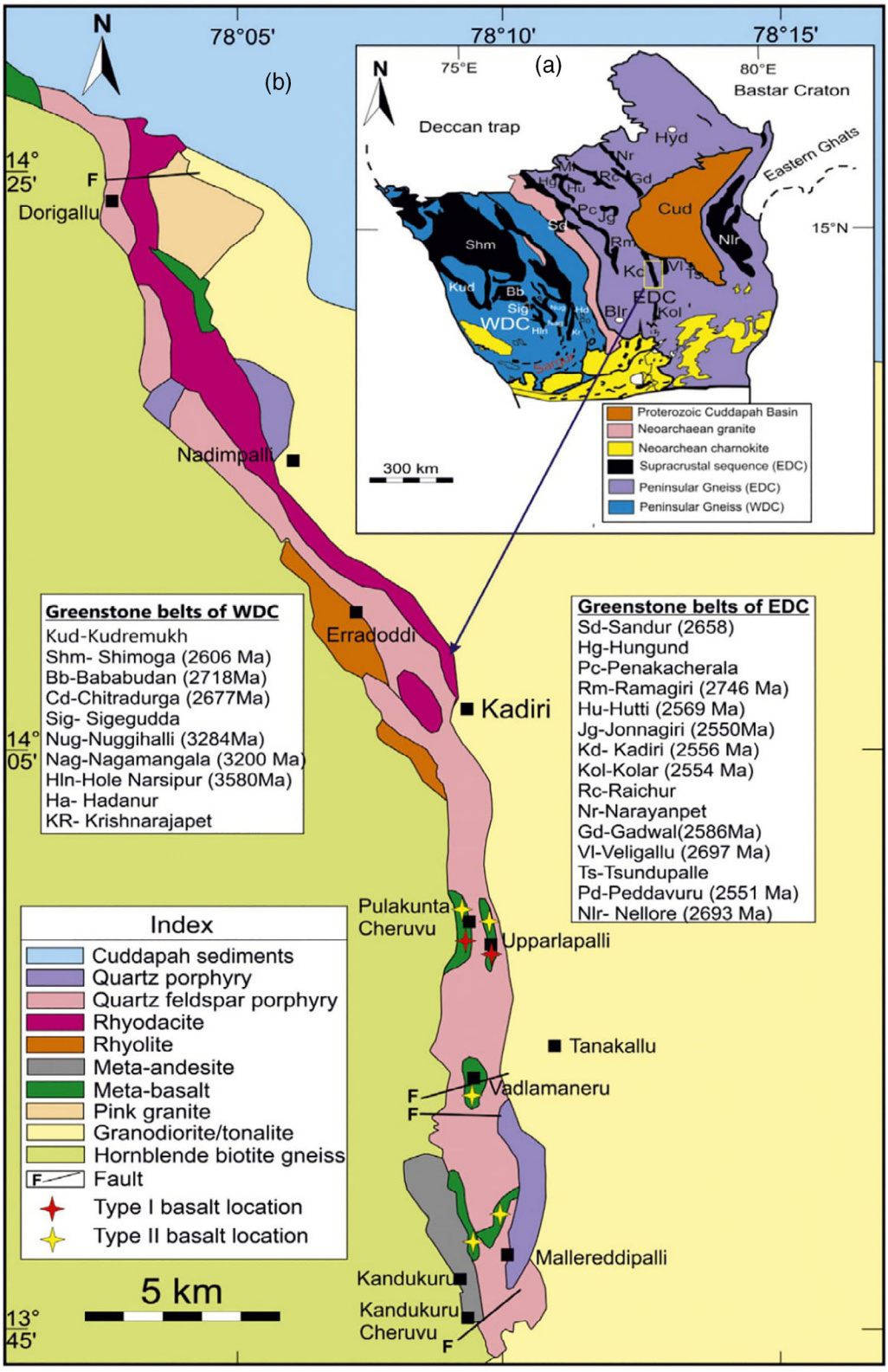


**FIGURE 1** (a) Inset figure is a simplified geological map of southern peninsular India showing the western and eastern Dharwar Craton, with the intervening belt of Closepet granites, the distribution of greenstone belts, and the study area (after Ramam & Murthy, 1997) and (b) simplified geological map of Kadiri greenstone belt (after Manikyamba et al., 2015) [Colour figure can be viewed at wileyonlinelibrary.com]

Bababudan Group unconformably overlying the migmatite with a basal oligomictic quartz-pebble conglomerate which is comparable in age to that of Rand (Africa). This oligomictic conglomerate of limited thickness consists of 90% framework clasts of resistant minerals and rocks, feebly radioactive and carries gold to a maximum of 0.25 g/t. Chitradurga Group of rocks constitutes a thick pile of volcano-

**TABLE 1** Simplified Precambrian stratigraphy of the Dharwar Craton (after Dey, 2013; this study)

| Western Dharwar Craton (WDC) | | Eastern Dharwar Craton (EDC) |
|---|---|---|
| Badami Group (0.6 Ga)<br>------Unconformity -------- | Kaladgi Group (~Cuddapah Supergroup) | Kurnool Group, Bhima Group (0.6 Ga)<br>------Unconformity -------- |
| BagalkotGroup<br>------Unconformity -------- | Dharwar Supergroup (2.9–2.6 Ga) | Chuddapah Supergroup (1.9–1.4 Ga)<br>------Unconformity--------- |
| Younger Granitoids (2.6 Ga)<br>*Chitradurga Group*<br>(conglomerate, quartzite, greywacke, pelite, BIF, and basalt | | TTG gneisses, granites (2.7–2.5 Ga), alkali granites (Kadiri)<br>*Kolar Group* (~2.7Ga), *Kadiri volcanics* (2.9–2.55 Ga)(basalts, komatiites, High-Mg basalts [Adakite], Pyroclaststic rocks, felsic volcanics, chert, BIF, metasediments) |
| *Bababudan Group* (conglomerate, quartzite, basalt, BIF<br>------Unconformity-------- | | |
| | | |
| *Sargur Group* (3.4–3.0 Ga; quartzite, pelite, calc-silicate, basalt, komatiite, BIF and layered mafic-ultramafics) | Gneisses (3.3–3.0 Ga) | Vestiges of older gneisses (~3.1 Ga) |
| *Gorur Gneisses* (~3.4 Ga) | | |

sedimentary unit comprising basalt, andesite, rhyolite, and tuffs along with a thick pile of greywacke sequence and banded iron formation (BIF). The Neoarchean rocks (2.8–2.5 Ga) of EDC are noted with three main lithological types, namely (a) Greenstone belt (GSB), (b) TTG, and (c) Calc-alkaline to potassic granitoids (Balakrishnan et al., 1999; Jayananda et al., 2000; Nutman, Chadwick, Krishna Rao, & Vasudev, 1996). The greenstone belts of EDC are preserved as narrow arcuate belts dismembered and intruded by granitoids of Late Archean ~2.5 Ga (Naqvi & Rogers, 1987). The ages of EDC are limited and mostly correlated with the Dharwar Supergroup (2.9–2.5Ga; Hokada et al., 2013) of the WDC. They have a bimodal age, 2.7 and 2.5 Ga recorded in mafic to felsic volcanism, and essentially felsic magmatism, respectively (Jayananda, Peucat, Chardon, Krishnarao, & Corfu, 2013; Sarma et al., 2008). There are about 12 GSBs in the western block and 14 detached greenstone belts in the eastern block of Dharwar Craton falling in the states of Karnataka and Andhra Pradesh. The GSBs of EDC are auriferous, and these are subjected to sinistral ductile deformation along eastern margins with the Late Archean granitoids (Drury et al., 1984). The greenstone belts of EDC have predominance of mafic and felsic volcanic rocks which are characterized as boninite, Nb-rich basalts, Mg-andesites, andesites, dacites, rhyolites, and adakites (Manikyamba et al., 2017 and references therein). Both Na and K-adakites have been reported from a number of greenstone belts (Manikyamba et al., 2020). One of the prominent features of EDC is the preservation of volcanic rocks commonly found at the convergent plate boundaries called subduction, typified by the Indus-Tsangpo Region (ITR) in the Himalayas often associated with gold mineralization. Some of these greenstone belts are deformed and engulfed by the gneisses, greenschists and upper amphibolite facies metamorphic assemblages (Ramakrishnan & Vaidyanadhan, 2008; Zachariah, Mohanta, & Rajamani, 1996).

## 2.1 | The Kadiri Volcanic Province

The NNW–SSE trending Kadiri greenstone belt of EDC (75 x 2.5 $km^2$), occurs in the southern part of the Kolar-Kadiri-Jonnagiri-Hutti composite greenstone terrane, and located south of the Mesoproterozoic Cuddapah Basin (Figure 1). The Kadiri belt comprises migmatite basement gneisses which are overlain by metabasic and intermediate to felsic volcanics (Kazmi & Kumar, 1991; Ramam & Murthy, 1997). Thin units of BIF occur above the felsic volcanics typifies lithostratigraphy of the Palaeoproterozoic Gwalior Basin in Central India (Chakraborty, Pant, & Paul, 2015). The Hutti-Jonnagiri-Kadiri-Kolar greenstone terrain is largest (~500 km) in dimension and contains gold mineralization which is being mined at Hutti at present. The enrichment of gold in the northern part of Hutti and southern end of Kolar indicate intra-oceanic island arc environment. The greenstone belts are traversed by trans-cratonic shear zones responsible for movements of hydrothermal fluids with gold-bearing mineralization (Chatterjee, Lingamurty, Singh, & Manikymba, 2013; Dey, Nandy, Chaoudhary, Yongsheng, & Zong, 2015; Dey, 2013; Manikyamba, Ganguly, Santosh, Singh, & Saha, 2015). One of the significant features of Kadiri belt is the predominance of felsic volcanic rocks over meta-basalts. Geochemical studies on Kadiri greenstone belt of EDC record occurrence of LREE-enriched and depleted basalts, Nb-rich basalts, Mg-andesites, dacites, rhyolite, and adakites (both sodic- and potassic-types) which reflect juvenile to mature stages of Neoarchean convergent plate margin processes much akin to that observed in Phanerozoic subduction systems such as Izu-Bonin-Mariana, Tonga-Kermadec, Kurile and Kamchatka arcs; New Britain and South Sandwich islands; Okinawa-Ryukyu and Baja California; Sunda-Banda arc, Mexico, Chile, and Aleutian Islands; Lesser Antilles; Setouchi volcanic belt, SW Japan; Mt. Shasta, northern California; Solomon Islands, Qiantang Terrane, Central Tibet

(Dey et al., 2015; Manikyamba, Ganguly, et al., 2014; Manikyamba, Saha, et al., 2014; Manikyamba et al., 2015, 2020). The mantle processes and geodynamic conditions involved in the evolution of Hutti-Jonnagiri-Kolar-Kadiri composite arc-back arc system generated magmas of diverse compositions and played a potential role for mineralization of noble metals, namely, gold (Au) tapped from a mantle refertilized and metasomatized by subduction components. The felsic volcanic units of Kadiri are represented by dacite, rhyolite including pyroclastic flow, a variety of tuff breccias, containing clasts of basalts, intermediate, and felsic rocks (Figures 2 and 3). Towards the south, near the western contact of the belt, thick and massive dacites and andesites are followed by porphyritic andesites which are interlayered with felsic volcanic rocks including massive rhyolites. Seven cycles of volcanic tuff breccia interlayered with dacitic/andesitic are identified at Kandukur village associated the outcrop (Figures 2 and 3). Tuff breccia has fragments of basalts and felsic rocks indicating post tectonic deformation (Figure 2). A variety of pyroclastic rocks and lava flows are encountered in KVP (Figures 2 and 3). The pyroclastic rocks are dominantly composed of tuff breccia with variable clasts dimensions of basement gneisses and granites or cognate fragments (co-magmatic, Fischer & Schmincke, 1984) of mafic or felsic volcanics. In these breccia, variable dimension of clasts with subtle orientation reflect on post-tectonic deformation (Figure 3). At places, large clasts of quartzo-felspathic rocks are observed. The variation in the dimension of the clasts within the tuff breccia which is cutting along three directions may reflect post consolidation deformation (Figure 3). These pyroclastic breccia of dacitic-rhyolitic compositions are deformed at many places indicative of post-volcanic deformation and commonly comprise lenticular, rim-type lapilli with a coarse-grained core surrounded by a fine-grained rim. These lenticular, rim-type lapilli reflect heat emanation, quenching, and flattening of drops of molten acidic lava that was ejected from an explosive volcanic eruption (Figure 3). Occasionally, bimodal massive lava consisting of xenoliths of felsic lava is observed (Figure 3). Such succession of tuff-felsic lava flows are identical to those observed in the Neoproterozoic and orogenic volcanic province of Malani rhyolites in western Rajasthan with alternations of tuff-rhyolite near Jodhpur (Bhushan & Chandrasekaran, 2002). The tuff breccias in which the clasts are stretched parallel to the foliation (Chatterjee, 2017; Dey et al., 2015; Manikyamba et al., 2020) suggest convergent margin magmatism and


**FIGURE 2** Field photographs of (a) mafic volcanics, (b) lapilli tuff, (c) Tuff breccia with fragments of basalts, and (d) Tuff breccia with linear alignment of fragments of basalt and felsic rocks, indicating post-tectonic deformation [Colour figure can be viewed at wileyonlinelibrary.com]


**FIGURE 3** Field photographs of (a) Tuff with clasts of variable dimension showing vague orientation, indicating post-tectonic deformation; the clasts are dominated by fragments of quartz, mafic volcanics, and quartzo-feldspathic rocks; (b) Large clasts of quartzo-feldspathic rock and lava flows in tuff; (c) Laminated tuff breccia with variable dimension of clasts showing post-consolidation deformation and lamination along three directions cutting each other; (d) Deformed pyroclastic breccia containing lenses of variable dimensions of felsic rocks tapering at both ends, (e) Tuff breccia containing lenticular lapilli with a rim around indicating cooling history and diagonal fractures cutting across the rock due to post-consolidation deformation, and (f) Bi-modal massive lava with lenses (xenolith) of fine-grained grey felsic lava [Colour figure can be viewed at wileyonlinelibrary.com]

fluid activity responsible for gold mineralization at Hutti (north of Kadiri) and Kolar (south of Kadiri) and uranium at Kadiri (Sreenivasulu, Padmasree, & Lakshmidevamma, 2013). Other rocks like lapilli tuffs, pumice (filled with secondary minerals), and pyroclastic flows (<1 m thickness) are less abundant. Eruption of lava flows (e.g., mafic volcanics, andesites, dacites, and rhyolites) followed the violent outburst of pyroclastic rocks (Figure 4). Presumably, the pyroclastic flows, containing welded tuffs are located close to volcanic vents and erupted

on cessation of the sub-aerial eruptions (tephras). The rocks were subjected to recrystallization and late deformation as noted by the orientation of lapilli, flow direction, and fine foliation in tuffs and lapilli stones. Apophyses of mafic volcanics in felsic lavas presumably mark the final phase of eruption at Kadiri. It may be mentioned in this context that the pyroclasts and felsic lavas are more abundant in the KVP over the mafic volcanics than any other greenstone belts in EDC (Table 2).


**FIGURE 4** Field photographs of (a) Rhyolites showing deformation; (b) contact between felsic lava and pyroclastic flow; (c) an andesitic lava flow cutting across the felsic volcanic rock; (d) a large outcrop of pumice indicating the rock may have been transported for long distances; (e) and (f) vesicular pumice filled by secondary minerals [Colour figure can be viewed at wileyonlinelibrary.com]

Three phases of folding have been recorded in the KVP. The $F_1$ folds are tight to isoclinal, show moderate plunge and associated with N-S to NNW-SSE prominent regional schistosity ($S_1$) and mineral lineation (Dey, 2013; Reddy & Jagadish, 1993). The second generation $F_2$ folds are open with variable plunge and generated crenulation cleavage. The third generation $F_3$ folds are open warps with ENE-WSW to E-W axial planes (Dey, 2013). The granitoids present at the eastern and western margins of the Kadiri belt are hornblende and biotite type (Chatterjee, 2017). Farther east and on the western side of this belt, the granitoids are massive, medium- to coarse-grained, pink and grey biotite granites (Dey, 2013; Manikyamba et al., 2015). The hornblende granitoids present at the eastern margin contains mafic, micro-granular enclaves which are stretched parallel to the foliation planes indicating syn-magmatic deformation of the enclaves whereas those in the eastern margin (away from belt) are highly deformed, sheared, mylonitized, and show ductile-brittle-sigmoidal deformations. At some places, the feldspar grains of the granitoids form lineation, which probably indicates magmatic lineation. The trend of the banding at some places is 170°-350° which follows the prolonged shear zone (Dey, 2013).

## 3 | TEXTURAL FEATURES

Petrographically, the mafic volcanic rocks are distinguishable from the metabasics (low temperature metamorphic equivalent) on the basis of abundance of mafic minerals, degree of recrystallization and texture. The latter contains quartz, feldspar, chlorite, biotite, and epidote and may be termed as 'greenschists' because of the preponderance of low-temperature minerals. The greenschists are characterized by lobate and cuspate structure indicating mixing of two magmas (Figures 4c and 5e). Presence of micrographic texture (mgp) suggests late crystallization of the studied mafic volcanics (Figure 5). The andesites contain quartz, plagioclase (often porphyritic and zoned), K-feldspar, amphibole, actinolite, biotite, and accessory minerals like epidote, sphene, ilmenite, magnetite, calcite, and zircon (Figure 6). The rock shows a variety of textures, such as flow, nematoblastic, porphyritic, mylonitic, and brittle deformation (Figure 7). Oscillatory or repeated or parallel zoning in plagioclase is common (Figure 7). Transformation of amphibole to biotite and in turn to chlorite apparently indicates cooling history of the magma. The rock has undergone low-grade metamorphism by occurrence of needles of actinolite cutting across the twinned planes of plagioclase (Figure 7; Table 3). In some sections, two types of amphiboles are also present (Figure 8). The quartz andesite contains laths of plagioclase, amphibole, biotite, and epidote with inclusions of alanite, whereas the biotite has inclusions of monazite and thorite (Figure 8). Occurrences of economic minerals like gold-silver, atomic minerals (monazite, thorite), rare-earths, titanium, magnetite, base metals, and pyrite are also recorded in the rock (Figure 9). The dacites are composed of quartz, plagioclase, recrystallized mafic minerals and minor components of ilmenite, magnetite, goethite, and haematite. Flow texture is most common, while minor presence of banded, intergranular, intersertal, and mylonitic textures are noticed, giving indication of direct crystallization of minerals from the melt (Figure 10). The rock shows post-tectonic cataclastic effects. Biotites dominate over the amphiboles reflecting on the cooling history of the rock. Plagioclase with exsolved quartz and K-feldspar, allanite at the core of epidote, allanite, and monazite in biotite, presence of bluish-green tourmaline and pink-coloured thorite are characteristic features of dacites (Figure 11; Table 3). Occurrence of modal muscovite in dacite gives unequivocal support of its derivation by partial melting of upper crustal rocks and suggests peraluminous composition. The dacites, on the other hand are noted with a wide occurrence of radioactive minerals, namely, monazite, thorite, and allanite, a source of thorium and uranium, used for generation of alternative source of electricity and nuclear weapons (Figure 11; Table 3). This study reports first time a potential source of atomic minerals from the felsic volcanic rocks (viz., andesites and dacites) from Kadiri (KVP), based essentially on petrographic study. Considering the significance of the new discovery, a systematic study of the mineral may be taken-up in future. The rhyolites have

**TABLE 2** Tectonic settings of the Hutti-Jonnagiri-Kadiri-Kolar greenstone belts, EDC (Manikyamba et al., 2015)

| Greenstone belt | Lithounits | Tectonic setting | Mineralization | References |
|---|---|---|---|---|
| Hutti | Depleted and enriched basalts, Mg-andesites | Plume-arc interaction | Abundant gold mineralization | 1, 2, 3 |
| Jonnagiri | Arc basalts, high-Mg basalts | Plume-arc interaction | Moderate gold mineralization | 4 |
| Kadiri[a] | Tuff breccia, lapilli tuff, pyroclastic flow, pumice, Arc basalts, NEB, adakites, felsic, and intermediate volcanics, alkali feldspar granite (A-type) | Subduction arc-back arc magmatism | Disseminated gold, uranium, thorium, rare-earths, titanium, and base metals | 5 |
| Kolar | Komatiites, high-Mg picritic basalts, arc tholeiites | Plume-arc accretion | Abundant gold mineralization | 6, 7, 8 |

*Note*: (1) Manikyamba et al. (2009); (2) Pal and Mishra (2002); (3) Giritharan and Rajamani (1998); (4) Saravanan et al. (2009); (5) Ramam and Murthy (1997); (6) Anantha Iyer et al. (1979); (7) Balakrishnan et al., (1999); (8) Rajamani et al. (1985).
Abbreviations: EDC, Eastern Dharwar Craton; NEB, Nb-enriched basalts.
[a]This study.

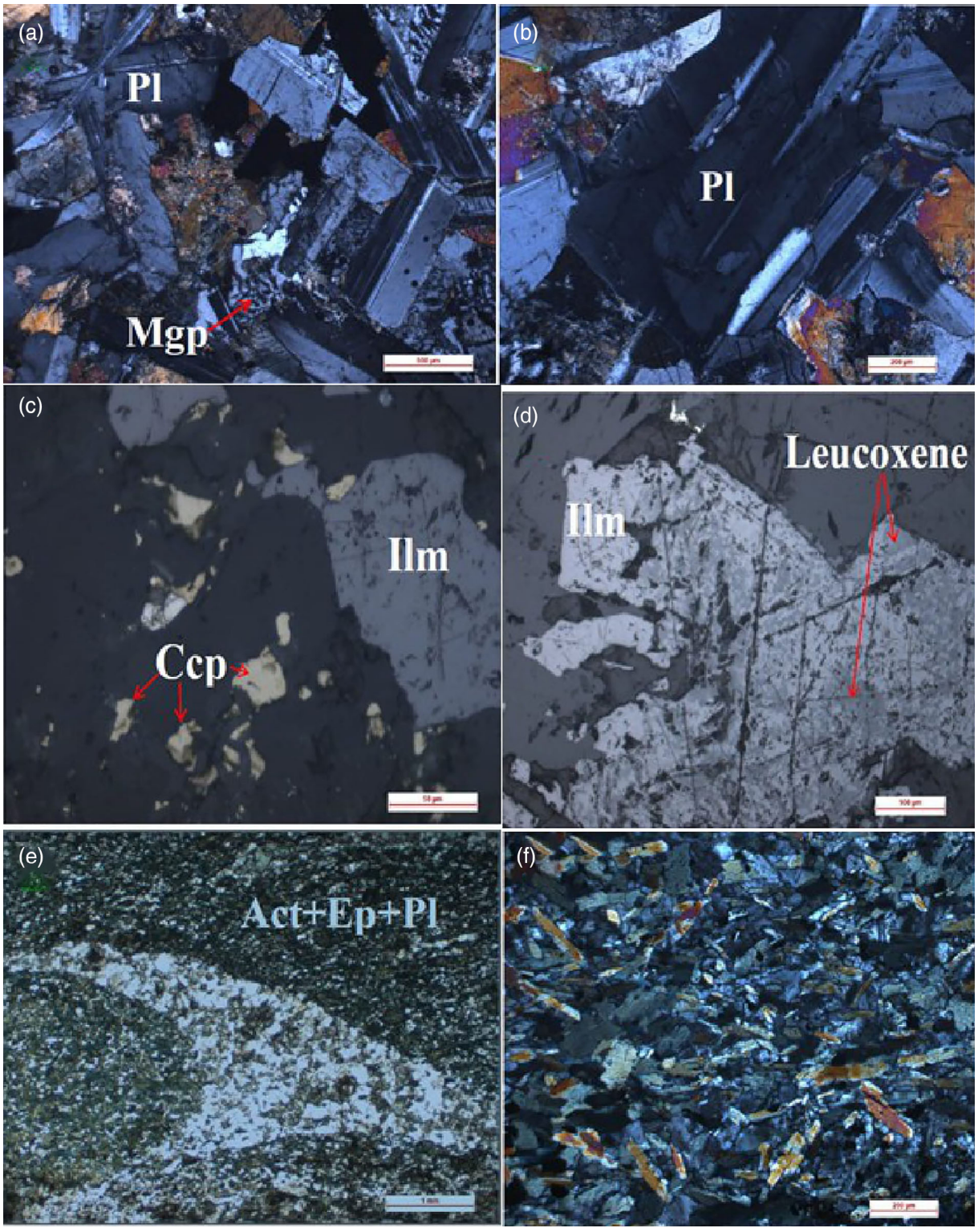


**FIGURE 5** Photomicrographs of basalts (a) showing intergranular to sub-ophitic textures. Development of micro-graphic pegmatites (Mgp), indicating derivation from highly fractionated magma. The plagioclases are mostly twinned and show normal zoning; (b) oscillatory zoning in labradorite; (c) ore minerals such as ilmenite-chalcopyrite, pyrite derived from late hydrothermal solution; (d) Magnified view of the formation of leucoxene after ilmenite in basalts under reflected light; (e) Lobate and cuspate structures indicating mixing of two magmas; and (f) variable orientation of minerals suggesting igneous protolith. Abbreviations: Act, actinolite; Ccp, chalcopyrite; Ep, epidote; Ilm ilmenite; Pl, plagioclase [Colour figure can be viewed at wileyonlinelibrary.com]

undergone high degree of shearing, ductile deformation and noted with strain shadow in quartz (Figure 12). Migration of grain boundaries in quartz due to shearing and exsolution of quartz in plagioclase are characteristic feature signifying its development under stress. Apart from quartz, both K-feldspar and sodic plagioclase are present. Secondary minerals such as chlorite after biotite and epidote after

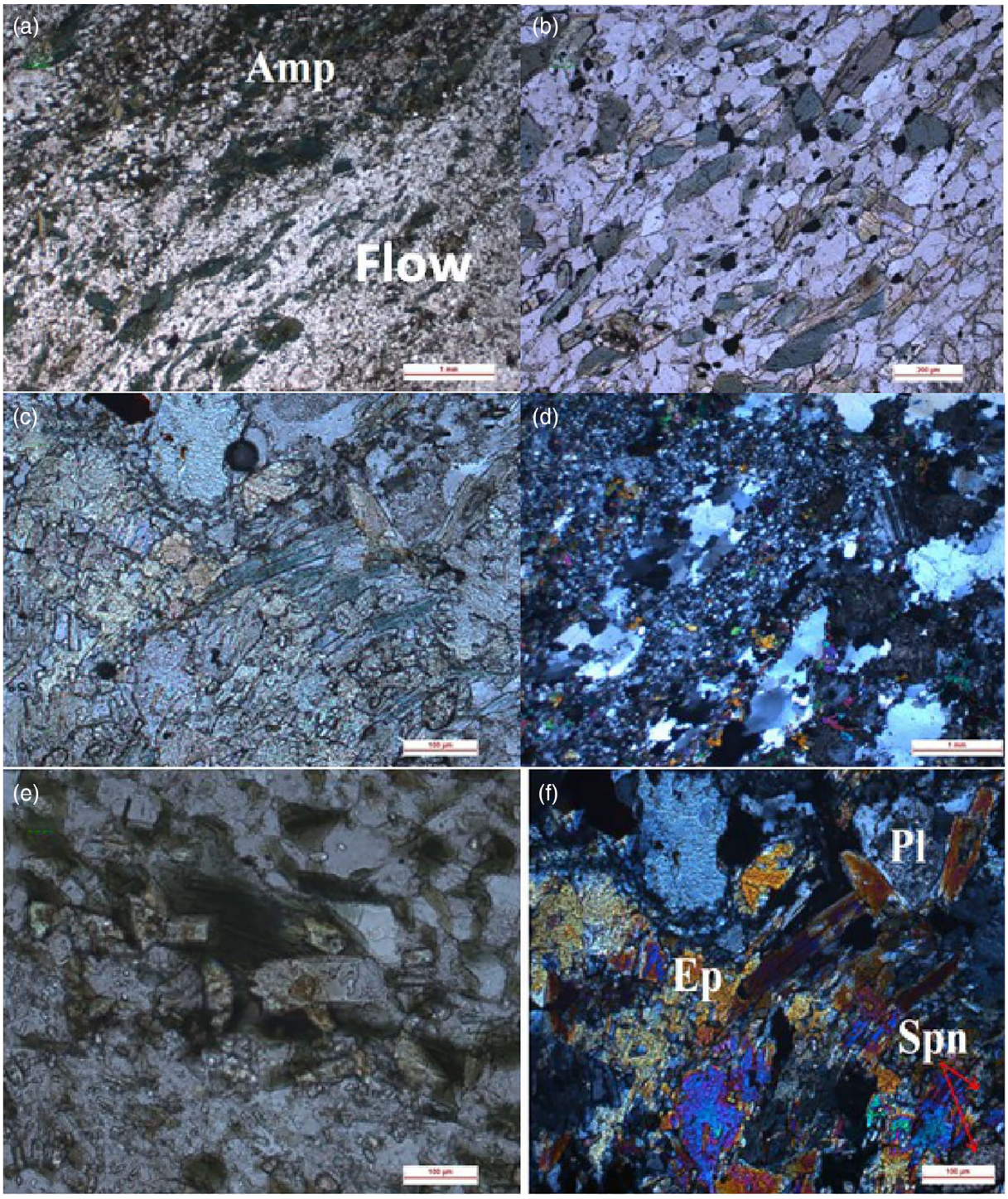


**FIGURE 6** Photomicrographs of andesite (a) Phenocryst of amphibole (Amp) in andesite in a mosaic of plagioclase and quartz. The flow texture is defined by alignment of amphiboles; (b) metablastic texture showing distribution of opaque minerals (ilmenite) along schistosity; (c) flow texture showing recrystallization with development of epidote and bending of long prisms of amphibole. Sphene and monazite occur as accessory minerals; (d) bimodal plagioclase in metamorphosed quartz andesite showing mylonitic texture with amphiboles (actinolite) along with epidotes; (e) alignment of biotites, amphiboles and epidotes imparting vague foliation. Phenocrysts of plagioclase cross cut the foliation and late to crystallize; and (f) strongly foliated meta-andesite containing amphibole, plagioclase (Pl), sphene (Spn), and epidote (Ep) [Colour figure can be viewed at wileyonlinelibrary.com]

plagioclase and minor opaque minerals are also observed. The 'Berlin blue' anomalous interference colour of the chlorite is identified as pennine, which characteristically occurs in palaeo-rhyolites (Figure 12; Pichler, Schmitt-Riegraf, & Hoke, 1997). It is grouped under orthochlorite of clinochlore group and formed by severe hydration of original mineral.

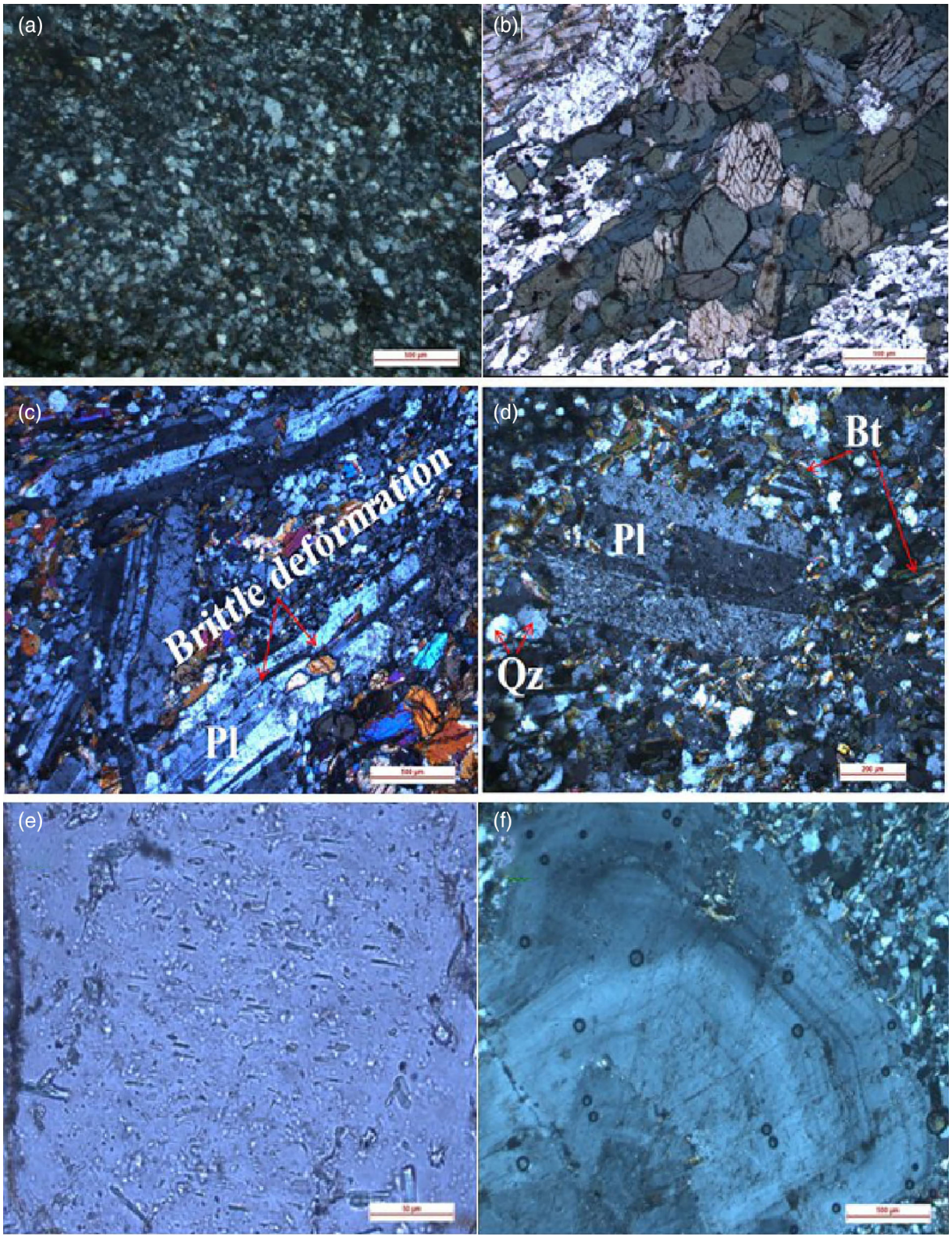


**FIGURE 7** Photomicrographs of andesite (a) Oscillatory zoning in plagioclase; (b) phenocryst of twinned plagioclase in quartz andesite surrounded by smaller grains of quartz, feldspars, and biotites; (c) actinolite needles cutting across the plagioclase phenocryst; (d) intergranular texture with brittle deformation in plagioclase in which the needles of actinolite cross-cut the zoned lamellae; (e) prismatic and basal sections; and (f) inequigranular texture predominantly consists of plagioclase [Colour figure can be viewed at wileyonlinelibrary.com]

**TABLE 3** Summarized account of geology and ore mineralization in the Neoarchean Kadiri volcanics (~2,700 Ma, EDC) based upon petrography

| S no. | Sample no. | Rock type | Texture | Primary minerals | Accessary minerals | Associated ores | Secondary minerals | Tectonic settings | Remarks |
|---|---|---|---|---|---|---|---|---|---|
| 1 | A12 | Basalt | Intergranular, micrographic (mgp) | Pl, Cpx | Bt, Il, Leuco | Base metals: Ccp sulphur and Gold: Py | Cpx → Bt, Il → Leuo | Subduction* | |
| 2 | A16 | Basalt | Intergranular, schistose | Pl, Amp | Ep | Opq | Ep, Chl | Subduction* | Cuspate and lobate structures, low – grade metamorphism |
| 3 | Several samples (felsic rocks) | Andesite | Fine-grained, flow texture, inequigranular, massif, intergranular, brittle deformation, xenomorphic granular | Qz, Pl, Amp > Bt, twinned and zoned Amp,Pl mostly phenocrysts, occasionally zoned with lamellar and oscillatory twinning | Ep, Mag, Ilm, Cal | *Noble metals*: Au, Ag<br>*Atomic minerals*: Mnz, Thr<br>*Base metals*: Ccp, Cv<br>*Titanium*: Ilm<br>*Gol*: Py<br>Iron:Mag, Gth | Amp → Bt, Chl | Subduction (Mg-andesites) – crustal accretion/fusion* | Fine needles of act across twinned lamellae of Pl, low-grade metamorphism |
| 4 | Several samples (felsic rocks) | Dacite | Fine-grained, flow texture, intergranular, banded, porphyritic | Qz, Fl, Bt ≥ Amp, zoned Amp, Cpx, Ms, Tur, Pl twinned: simple and lamellar | Ep, Chl | *Atomic minerals*: Aln, Mnz, Thr<br>*Titanium*: Ilm<br>*Iron*: Mag | Chl, Gth, Hem | Crustal accretion (QADR – fusion of upper crust) | Pl with exsolved qtz, Aln at the core of Ep |
| 5 | A 18 | Rhyolite | Flow texture, shearing, ductile deformations, strain shadow in quartz | Qz, Fl | Opq, Chl, Ep | | | Crustal accretion/fusion | Chl with 'Berlin blue' interference colour, Exsolution of Qz in Pl, Migration of grain boundary in Qz due to shearing |
| 6 | A4 | Alkai Granite | | Qz, Fl, Perthite, Bio > Amp | Ap, *Zr*, Ep | Opq | | Arc orogeny/ rifting | Shearing together with heating along shear zones. Strain shadow and grain boundary migration in Qz |

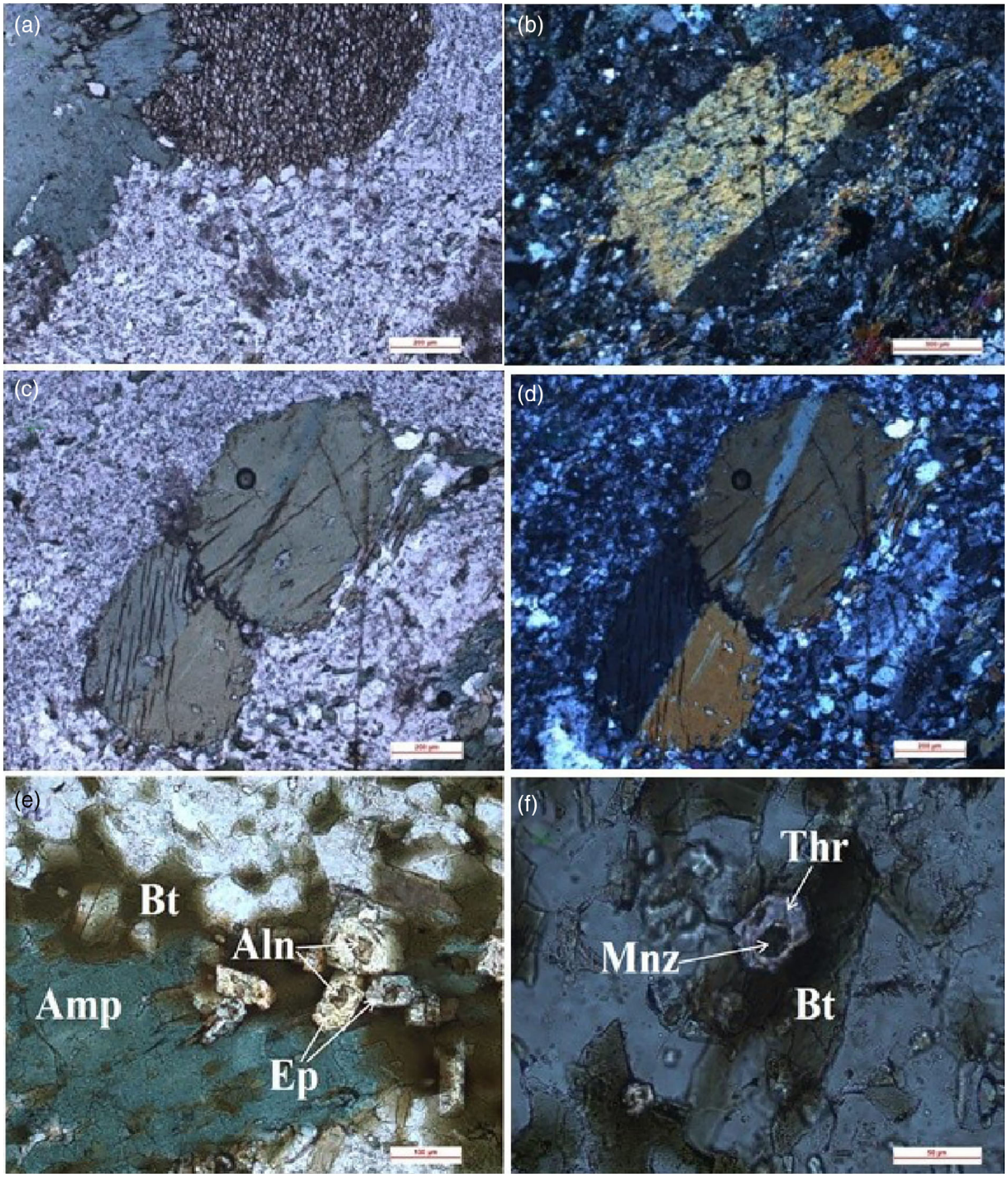


**FIGURE 8** Photomicrographs of andesite (a)–(d) Phenocrysts of two types of amphibole along with twinning; (e) Quartz andesite containing laths of plagioclase, amphibole, biotite, and epidote with inclusions of allanite (Aln); and (f) Quartz andesite with monazite-thorite (Mnz-Thr) association within biotite with radial cracks and pleochroic halos [Colour figure can be viewed at wileyonlinelibrary.com]

A special variety of granite termed as peralkaline granites in which plagioclase is <10% of the total feldspar and quartz is >10% by volume. It usually occurs in rift zones and considered to be anorogenic. These are mildly alkaline granites with low CaO and $Al_2O_3$. It is characterized by the occurrence of alkali feldspar, microperthite, and albite, hence termed as subsolvus type containing both alkali feldspars (orthoclase or microcline or microperthite) and discreet grain of albite. It is a medium-grained rock, composed essentially of quartz, K-feldspar, microperthite, albite, and ferromagnesium minerals like amphibole, biotite, chlorite, and epidote. Resorbed quartz and perthites occur as phenocrysts, while the ferromagnesium minerals are situated in the inter-spaces of larger grains (Figure 13). Highly resorbed elongated quartz show strain shadow and grain boundary migration (Figure 13). The alkali feldspar consists of sodic plagioclase (extinction angle 8°) and microcline and/or microperthite, biotite, apatite, and epidote with crude

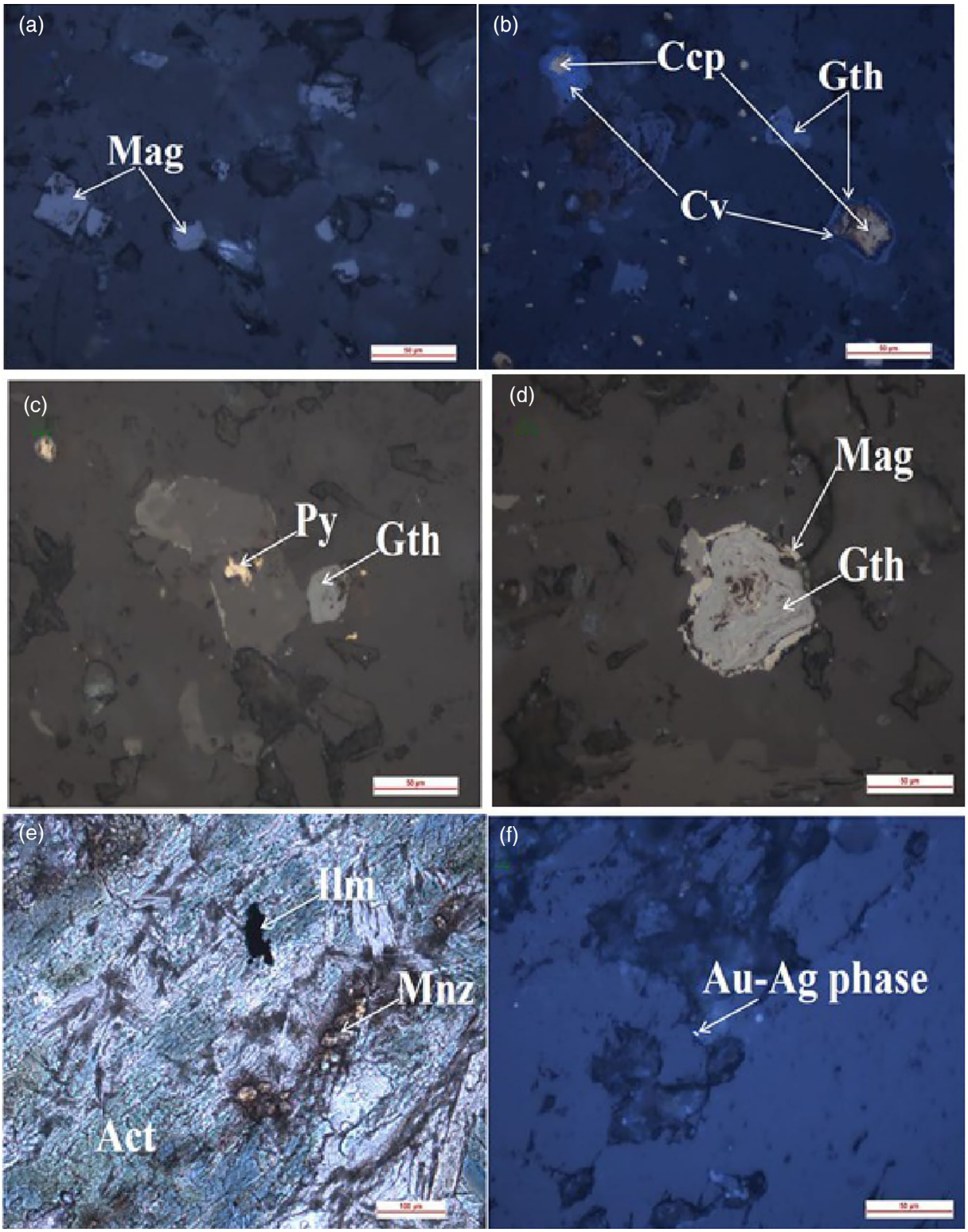


**FIGURE 9** Photomicrographs of andesites with ore minerals (a) Euhedral magnetite (Mag); (b) Chalcopyrite-covellite-goethite (Ccp, Cv, Gth); (c) specks of chalcopyrite-pyrite-goethite; (d) goethite showing colloform banding surrounded by magnetite and haematite; (e) monazite and ilmenite occurring along foliation plane; and (f) gold and silver phases occurring in close association of base metal sulphides [Colour figure can be viewed at wileyonlinelibrary.com]

foliation in hornblende-biotite alkali-feldspar granites. The apatite occurs as bulbous grains instead of typical idiomorphic form (Figure 13). It shows distinctive first order interference colour and straight extinction. The mineral is rimmed with altered biotite (chlorite) flakes. The sodic plagioclase (albite) contains inclusions of biotite. A few grains of zircon (25 μm; Figure 13), present in this rock

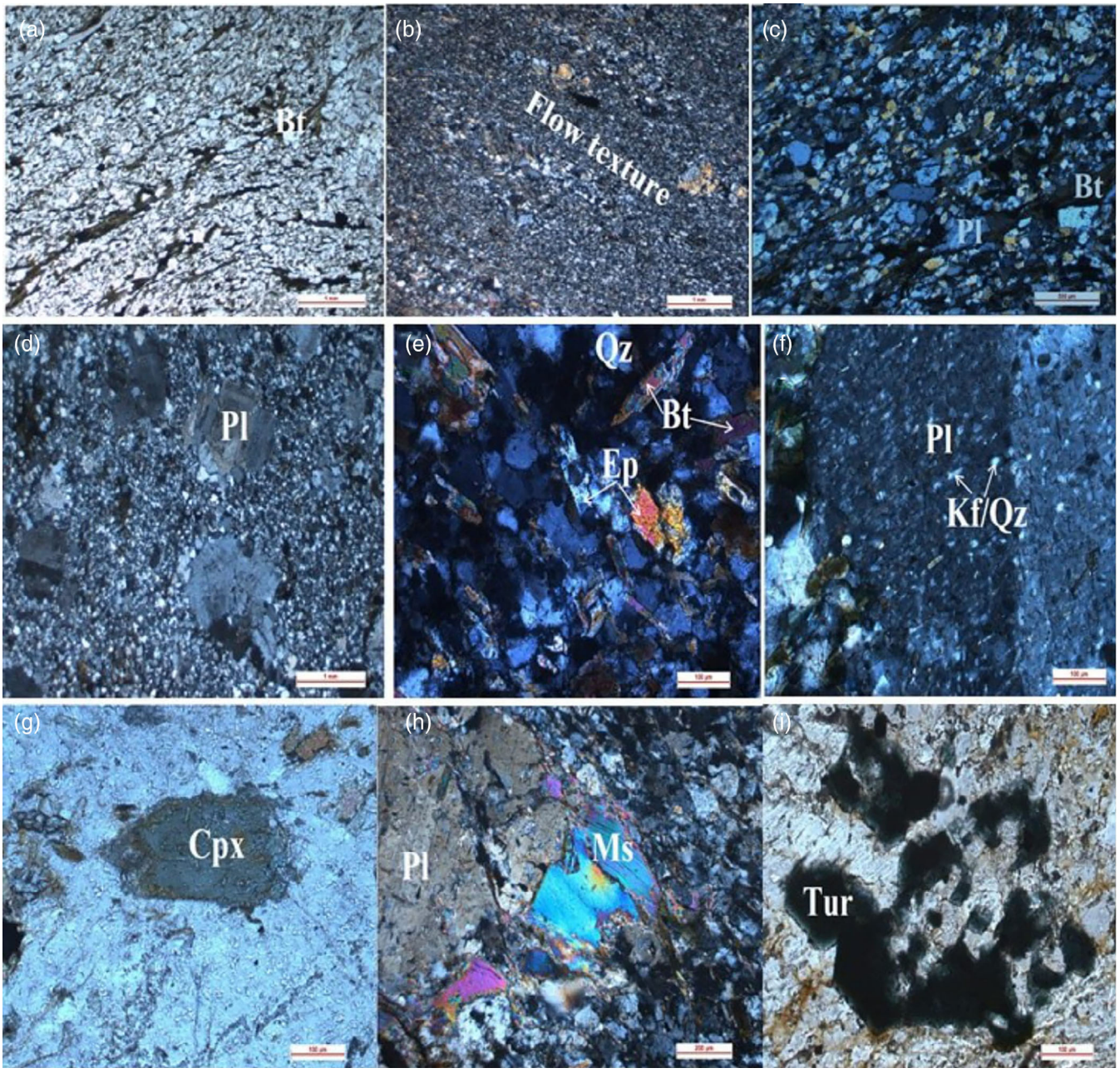


**FIGURE 10** Photomicrographs of dacites (a)–(c) flow texture superimposed by foliation of biotite and with parallel bands of felsic components; (d) mylonitic texture with plagioclase phenocrysts in fine-grained groundmas of quartz and feldspars in which the latter shows cataclastic effects; (e) intersertal texture with biotite, epidote, quartz, and feldspar; (f) phenocryst of plagioclase with exsolved quartz, feldspar, and biotite; (g) bluish green clinopyroxene (Cpx) phenocryst showing resorption in quartzo-feldspathic groundmass suggestive of late crystallization (AFC); (h) Plagioclase, muscovite (Ms), and biotite indicative of peraluminous composition of magma; (i) zoned tourmaline (Tur; indicolite) with iron and manganese as one of the components formed during late stage hydrothermal crystallization as pneumatolysis or gaseous emanations from volcanic vent [Colour figure can be viewed at wileyonlinelibrary.com]

endorse that the parent magma was formed through partial melting of crustal rocks.

## 4 | GEOCHEMICAL ATTRIBUTES

Average primitive mantle contains 18 ppb uranium and 64 ppb thorium and fluid-fluxed addition of uranium under oxidizing conditions can therefore elevate U/Th ratios into the range observed in island arc magmas. Hence, fluid-driven uranium cycling during incipient stages of Archean subduction and consequent U enrichment in arc magmas substantiate the role of oceanic plate subduction and fluid-controlled elemental cycling in triggering palaeo-ocean oxygenation. Therefore, it can be envisaged that the U–Th systematics of arc magmas generated in Archean subduction regimes were explicitly mediated by fluid-driven mobilization of U and addition of U-rich

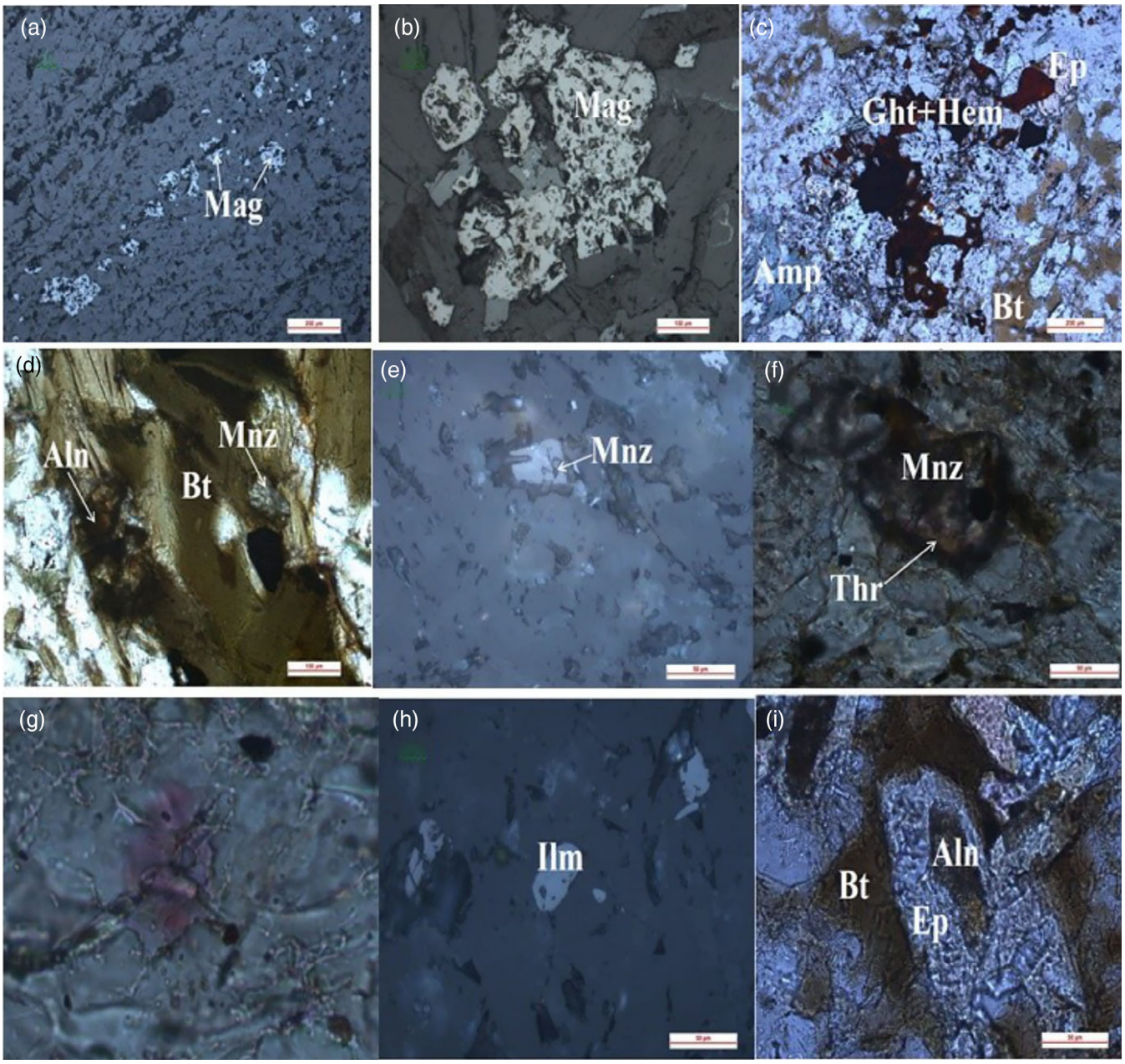


**FIGURE 11** Photomicrographs of dacites with ore minerals (a) Orientation of magnetite grains along flow direction; (b) aggregate of magnetite grains; (c) development of secondary minerals goethite-haematite-amphibole-epidote-biotite due to hydrothermal alteration during late crystallization; (d) occurrence of allanite-monazite within brownish-green biotite which are aligned along the flow direction; (e) occurrence of monazite; (f) occurrence of monazite-thorite in altered biotite; (g) pink thorite in dacite; (h) presence of Ilmenite; and (i) occurrence of allanite in the core of epidote. The latter is surrounded by a rim of biotite [Colour figure can be viewed at wileyonlinelibrary.com]

fluids from slab to mantle under oxidizing condition during initial stage of subduction and post-eruptive submarine hydrothermal alteration causing secondary loss of U and increasing Th (Manikyamba et al., 2017). In terms of Th/Ta versus Yb variations (Figure 14a), the felsic volcanic rocks from Kadiri comprising rhyolitic and dacitic compositions straddle the fields for oceanic arc and active continental margin. The affinity for an active ocean-continent convergence setting is more pronounced in Figure 14b owing to elevated abundances of Th over Ta. This Th enrichment can be equated in terms of intra-crustal melting and assimilation of continental crust by subduction-derived basaltic magmas at active continental margin setting. The volcanic agglomerates from Kadiri share the geochemical signatures and tectonic affiliation of the felsic volcanic rocks and show pronounced LREE/HREE fractionation with distinct HFSE depletion and Th enrichment (Figure 14c,d; Manikyamba et al., 2020). The geochemical attributes of felsic volcanic rocks from KVP reflect distinct LREE enrichment over HREE with elevated abundances of Th and U (Table S1) which collectively endorse metasomatism of the sub-arc

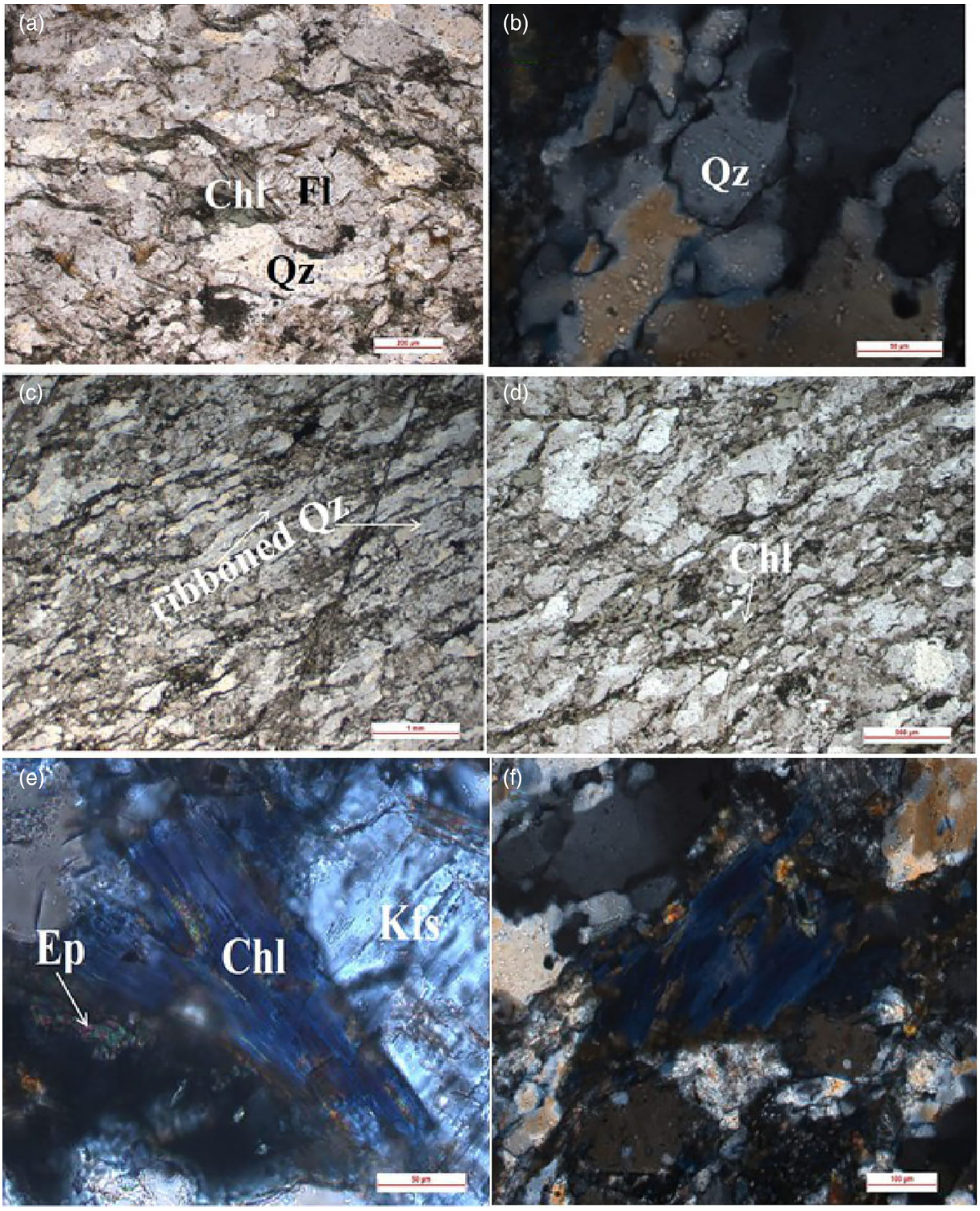


**FIGURE 12** Photomicrographs of Rhyolite (a) Porphyroclasts of quartz (50–60%) and feldspars (30%) with chlorite as slivers in the transformation of biotite during dynomo-thermal metamorphism; (b) grain boundary migration in quartz ('tectonite'), developed under extreme dynamo-thermal metamorphism; (c) finely foliated sheared rhyolite with ribbon quartz; (d) sheared rhyolite with ductile brittle deformation showing marginal granulation, strain shadow, stretching and elongation of quartz and feldspars; (e) twinned K-feldspar (Kfs), quartz, epidote, and chlorite with anomalous Berlin blue interference colour; (f) resorption of quartz and feldspars reflecting on cataclastic effect and plastic deformation and grain size reduction caused due to differential stress. Anomalous Berlin blue interference colour of chlorite (*pennine*) associated with epidote and biotite [Colour figure can be viewed at wileyonlinelibrary.com]

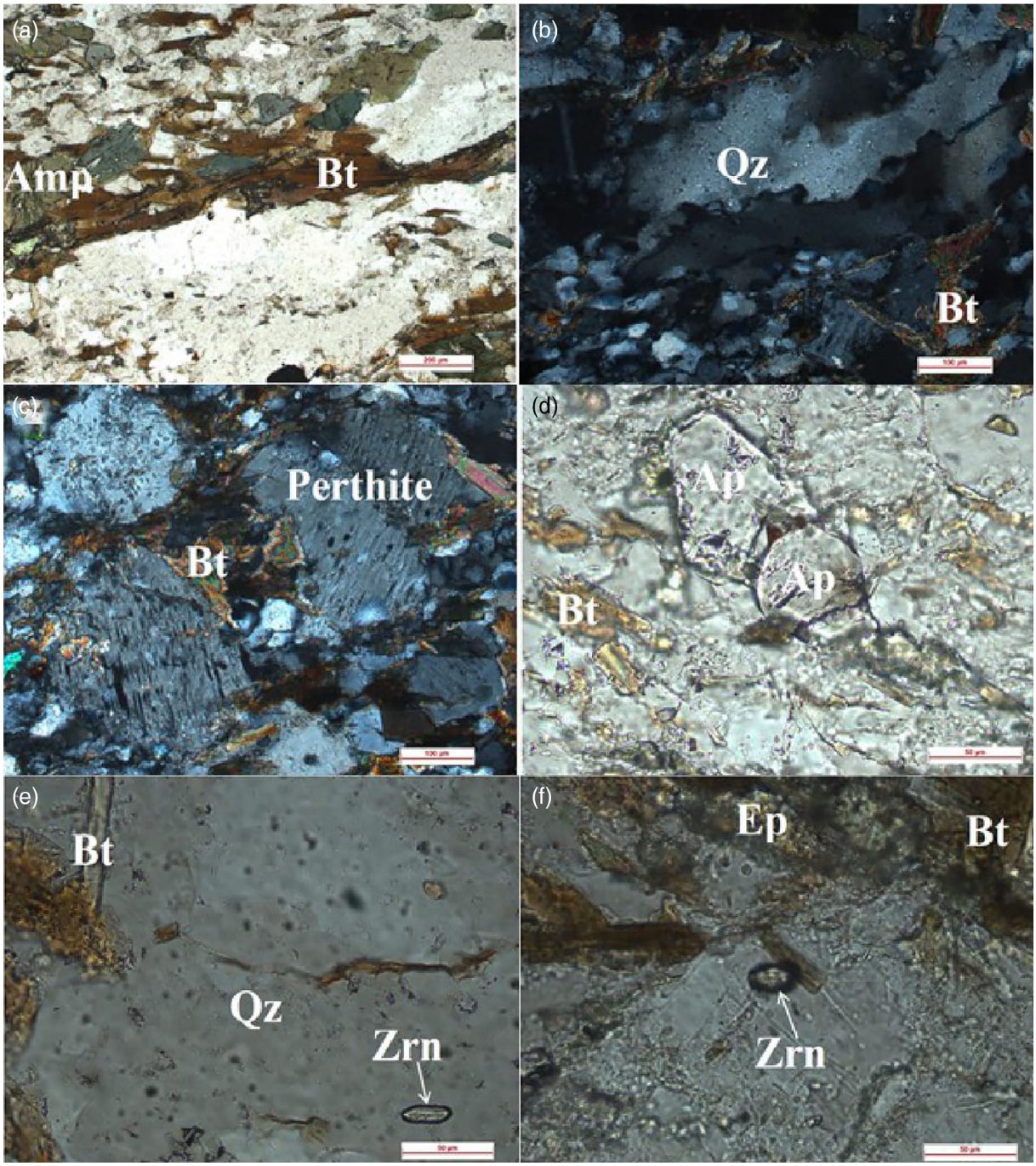


**FIGURE 13** Photomicrographs of alkali feldspar granite (a) quartz, feldspar, amphibole, biotite, and epidote; (b) highly resorbed elongated quartz showing strain shadow and grain boundary migration in association with feldspar and biotite; (c) resorbed quartz and perthite occurring as phenocrysts along with mafic minerals viz., biotite, chlorite and epidote occurring at the interstices of larger grains; (d) sodic plagioclase biotite, apatite (Ap) and epidote imparting foliation direction; (e) biotite and zircon (Zrn) (25 μm) in association with quartz; and (f) feldspar, biotite, zircon, and epidote in association with feldspar [Colour figure can be viewed at wileyonlinelibrary.com]

mantle by fluid influx from dehydrated oceanic slab. Rhyolites, dacites, and volcanic agglomerates of Kadiri Volcanic Province (KVP) show uniform HREE (Yb) depletion with negative Eu anomalies and a transitional composition marked by depleted to enriched Th and Zr concentrations (Figure 14a,b,d). These observations implicate parent melt generation with garnet in the residue, plagioclase fractionation, and a geodynamic transition from ocean–ocean to ocean–continent convergence.

## 5 | MINERALIZATION

### 5.1 | Gold

Major occurrences of gold in Archean are restricted to ~2.7 Ma age. Hence, the geological set up is ideal in the greenstone belts of the Dharwar Craton which is hosted in the metabasalts, andesites (Gadag,

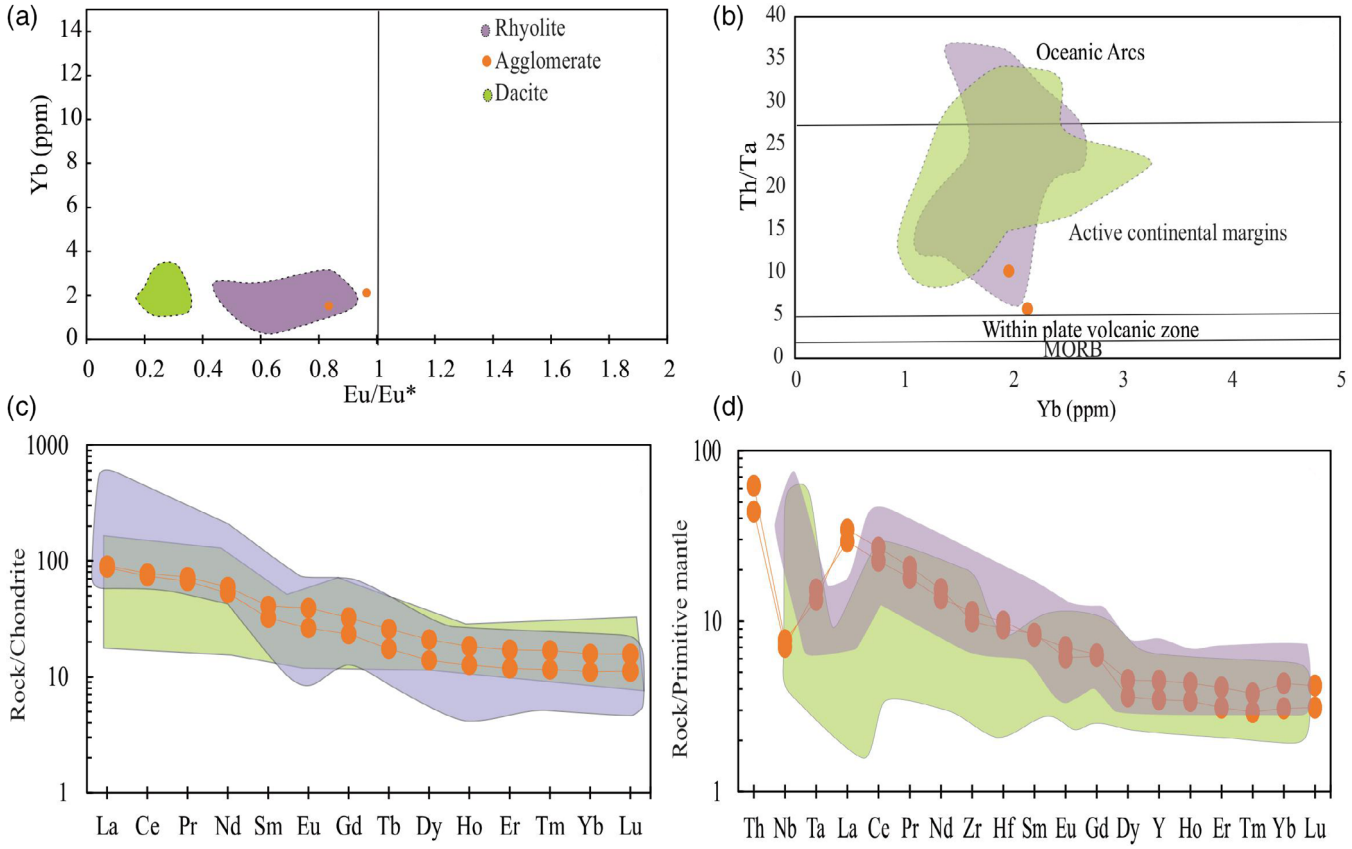


**FIGURE 14** (a) Th/Ta versus Yb relationship in which felsic volcanic rocks of Kadiri are straddling the fields of oceanic arc and active continental margin; (b) enrichment of Th over Ta indicative of ocean-continent convergence; (c) and (d) volcanic agglomerates from Kadairi show pronounced Light rare earth elements (LREE) / Heavy rare earth earth elements (HREE) fractionation with distinct High filed strength elements (HFSE) depletion and Th enrichment [Colour figure can be viewed at wileyonlinelibrary.com]

Kolar, Veligallu, Hutti, Ramagiri, etc.) felsic volcanics (southern part of Kolar gold field), and in sedimentary rocks such as greywacke (Sangli-Mysore mine, Attikatti-Kabuliyankatti) and BIF (Ajjanahalli and Chinmulgund). The gold mineralization is not restricted to any single lithological unit but occur in a wide variety of rock types. Manikyamba, Naqvi, et al. (2004) reported the orogenic gold occurrence in the Penakacherala greenstone belt in EDC and discussed the role of subduction-derived fluid processes towards genesis and precipitation of gold. Sarma et al. (2008) suggested the age of the gold deposit and associated xenotime of Gadag area. Minor occurrence of gold is noticed in granitoids present at its contact with the schist belt (Unpublished Report, GSI). Controlling factor for the mineralization of gold is the structural control as exemplified by ductile/brittle shears, fold closures and contacts of lithounits sited adjacent to transition shear zones. The shear control for gold mineralization is very evident in Kolar, Hutti, Ramagiri, and Veligallu greenstone belts (Manikyamba, Kerrich, Naqvi, & Ram Mohan, 2004). In the Ajjanahalli belt, in addition to shear, antiformal hinze zones have played a dominant role in controlling the gold mineralization and the isotopic and geochemical studies reveal the mantle source is responsible for this auriferous fluid (Sarangi, Srinivasan, & Balaram, 2013; Swain et al., 2018). In the Chinmulgund area, mineralization is at or near the contact of BIF with pyritic tuff. The gold mineralised zone is identified by wall rock alteration exemplified by retrogression of minerals and influx of potash into the wall rock (chloritization and sericitization). In addition, mineralised zones are invariably associated with sulphide minerals like pyrite, pyrrhotite, chalcopyrite, galena, and arsenopyrite. Carbonization is also present in several instances. Likewise, LILE-LREE enrichment and occurrence of gold in amphibolite-gabbro-TTG-charnockite suite from Nilambur region of the Wynad Gold Belt in the Southern Granulite Terrain (SGT) have been attributed to mantle metasomatism, active subduction–accretion processes during Archean-Proterozoic transition (Shaji et al., 2014).

## 5.2 | Atomic minerals: Uranium and rare-earth minerals

The felsic rocks are noted with frequent occurrences of thorium, monazite, and allanite, known as source of thorium, uranium, and REEs. Monazite occurring in such dacites is a major source of REE like cerium (Ce), lanthanum (La), neodymium (Nd), and Yttrium (Y), contributing 50–60% of REEs. Similarly, presence of thorite ($ThSiO_4$) in dacite, a metamict mineral, is strongly redioactive and contains

normally up to 10% uranium. Recent exploration by Air *Thorium* Borne Mineral Survey carried out by the Geological Survey of India and established a Th–U anomaly confined to a narrow shear zone running between south of Bangalore and Penikunda in Andhra Pradesh in the N-W and traced up to the KVP. The felsic volcanic rocks of KVP such as andesites and dacites containing atomic minerals, uranium, thorium, and REE should be given proper attention in future studies.

## 6 | DISCUSSION

The main gold-bearing greenstone belts of EDC are Ramgiri-Penakacherla-Jonnagiri schist belt and a number of old workings for gold are present at Ramapuram and Bhadrampalli in Penakacherla area; Chennabhavi, Yeppamana, Ompratima-Ghantalappa and Jibutil in Ramagiri, which gives testimony of the presence of gold (Manikyamba, Kerrich, et al., 2004). The old workings (mines) followed the ductile-brittle shear zones and confined to highly altered metabasalts which cuts at an angle to the foliation in en-echelon pattern. The metabasalts are massive to schistose in nature and metamorphosed to greenschist facies and were subjected to shearing and faulting. These rocks are in tectonic contact with granodiorite/tonalite to the east, and hornblende/biotite granite to the west (Dey et al., 2014, 2015). The granitoids are part of the Peninsular Gneissic Complex (Naqvi & Rogers, 1987) and considered to be intrusive into the belt. The source of gold is related to mantle source connected to deep fractures (>200 km depth), which paved an easy passage of magma to move up on partial melting of peridotites, tapping the siderophile elements (Au–Ag) that are preferentially enriched in the nickel-iron core.

Although the relative distribution of gold varies, most of the greenstone belt lithologies of EDC are gold-bearing among them Kolar, Hutti, Ramagiri, Penakacherla, and Jonnagiri are worth mentioning. The Neoarchean period (2.8–2.7 Ga) was marked by a peak in crustal growth, enhanced crustal thinning and extension, development of thick komatiite-basalt and felsic volcanic sequences, large scale deposition of BIFs, cratonization, regional deformation and metamorphism, and development of shear zone systems represents an important timeframe in greenstone metallogenesis (Ganguly et al., 2016; Manikyamba et al., 2017. Mishra, Pruseth, Hazarika, and Chinnasamy (2018) provide a detailed account of the nature and source of ore-forming fluids contributing to the genesis of Neoarchean orogenic gold deposits associated with the granite-greenstone belts of Dharwar Craton. Orogenic gold mineralization associated with Archean granite-greenstone terranes is primarily controlled by structural style, tectonic setting, metamorphism of host and associated rocks, shear zones, hydrothermal system involving physico-chemical processes and flow of hydrothermal fluids for mobilization, transportation, and deposition of gold. Geochemistry of sulphide, tourmaline and other minerals, and also fluid inclusion microthermometric and Raman spectroscopic data to yield important constraints on the source of ore fluid, nature of gold transport and mechanism of gold ore formation in the Dharwar Craton. An uniform ore fluid compositions in orogenic gold deposits of Dharwar Craton and their origin from low salinity, reduced aqueous-gaseous fluids derived by hydrothermal alteration and metamorphic devolatilization of mafic rocks and interlayered sediments of Dharwar greenstone belts has been envisaged. It has been propounded that gold precipitation occurred by fluid-rock sulfidation reactions in narrow P–T regime and fluid phase separation driven by fluid pressure fluctuation. Thus, it can be inferred that the pervasive and recurring subduction–accretion orogenic events, juvenile crust generation, crustal reworking and recycling, fluid-fluxes and mantle refertilization during Neoarchean played a pivotal role in the Au–U–Th–REE mineralization. The mineralogical and geochemical features of volcanic supracrustals of KVP endowed with prominent abundances of gold, U–Th and REE adheres to this consensus and stands out as a potential archive of Neoarchean accretionary orogens and associated Au–U–Th–REE mineralization processes.

## 7 | CONCLUSIONS

The present study reveals multi-metal mineralization associated with the Kadiri volcanics (Table 3). Viable deposits of gold should be traced in the metabasalts close to the vicinity of ancient findings of gold apparently controlled by tectonism. The affinity of gold in rocks with high-Mg is natural for its localization. Unlike the Kolar belt which is known for the occurrence of basaltic komatiite with spinifex texture of olivine, equivalent to mantle peridotite, the KVP is devoid of such rocks. However, small occurrences of Nb-rich basalts, high-Mg andesites that are derived at plate convergence and Mg-rich adakites generated by melting of the subducted plates may be looked for gold. Dominance of felsic rocks over mafic volcanics at KVP with very limited or insignificant volume of sedimentary supracrustals, the authors have made a detailed investigation in reflected light of felsic units with great success. Further studies may be taken up to establish the concentration of gold and atomic minerals in the mafic and felsic rocks of KVP.

## 8 | RECOMMENDATIONS

A systematic study of KVP with special thrust on mineralization of gold and other economic resources is recommended. Creation of large scale map for geophysical and geochemical study and prospecting of atomic minerals are yet to be taken up. Earlier works focussed mainly on geochemical and isotopic studies that are useful for identification of tectonic settings and origin of magma (crust–mantle source). It is recommended that systematic study of volcanic rocks and associated granites be taken up dealing with petrography, ore microscopy, EPMA, geochronology, and fluid inclusions to establish the tectono-magmatic history and mineralization of these rocks. Similarly, geophysical studies and prospecting of atomic minerals may be carried out tracing the locales of ore mineralization and their source.

Application of recent geophysical and geochemical techniques with 3D projection of data and superimposition of the same on

geological map may be taken up. This will help to identify geochemical anomaly for location of gold and other minerals at different levels of a mine. Integration of field and laboratory data may be taken up for further exploration.

## ACKNOWLEDGEMENTS

The authors are thankful to Dr. V.M. Tiwari, Director, CSIR-NGRI for permitting to publish this work. NGC acknowledges the help of Geological Survey of India, Bangalore for providing the microscope facility and is highly thankful to M. Shareef for fruitful discussions during the preparation of the article. Two anonymous reviewers are gratefully acknowledged for their incisive reviews which significantly enhanced the quality of our manuscript C. Manikyamba acknowledges the financial help from MLP 6406-28 (C.M.) project funds and Department of Science and Technology, India (ST SR/S4/ES-510/2010). S. Ganguly acknowledges DST-INSPIRE Faculty project (IFA14-EAS-25) for financial support. Arijit Pahari and C. S. Sindhuja acknowledge the DST INSPIRE fellowship for pursuing the PhD programme at NGRI. Drs. Keshav Krishna and M. Satyanarayanan are thanked for providing the geochemical data.

## ORCID

*Chakravadhanula Manikyamba* https://orcid.org/0000-0003-4736-4306

*Sohini Ganguly* https://orcid.org/0000-0003-0097-6911

## REFERENCES

Anantha Iyer, G. V., & Vasudev, V. N. (1979). Geochemistry of the Archean metavolcanic rocks of the Kolar and Hutti gold fields. *Journal of Geological Society of India*, *20*, 419–432.

Balakrishnan, S., Rajamani, V., & Hanson, G. N. (1999). U–Pb ages for zircon and titanite from the Ramagiri area, southern India: Evidence for accretionary origin of the eastern Dharwar Craton during the Late Archaean. *Journal of Geology*, v, *107*, 69–86.

Banfield, J. F., & Eggleton, R. A. (1989). Apatite replacement and rare earth mobilization, fractionation, and fixation during weathering. *Clays and Clay Minerals*, *37*, 113–127.

Bea, F. (1996). Residence of REE, Y, Th and U in granites and crustal protoliths; implications for the chemistry of crustal melts. *Journal of Petrology*, *37*, 521–552.

Berger, A., Janots, E., Gnos, E., Frei, R., & Bernier, F. (2014). Rare earth element mineralogy and geochemistry in a laterite profile from Madagascar. *Applied geochemistry*, *41*, 218–228.

Bhushan, S. K., , & (2002). Geology and geochemistry of the magmatic rocks of the malani igneous suite and tertiary alkaline province of Western Rajasthan. *Geological Survey of India Memoir*, *126*, 1–181.

Braun, J. J., Pagel, M., Herbilln, A., & Rosin, C. (1993). Mobilization and redistribution of REEs and thorium in a syenitic lateritic profile: A mass balance study. *Geochimica et Cosmochimica Acta*, *57*, 4419–4434.

Chadwick, B., Vasudev, V. N., & Hegde, G. V. (2000). The Dharwar Craton, southern India interpreted as a result of Archean oblique convergence. *Precambrian Research*, *99*, 91–111.

Chakhmouradian, A. R., & Wall, F. (2012). Rare earth elements: Minerals, mines, magnets (and more). *Elements*, *8*, 333–340.

Chakraborty, P. P., Pant, N. C., & Paul, P. P. (2015). In R. Mazumder & P. G. Eriksson (Eds.), Precambrian basins of India: Stratigraphic and tectonic context *Controls on sedimentation in Indian Palaeoproterozoic basins: Clues from the Gwalior and Bijawar basins, Central India* (Vol. 43, pp. 67–83). London, England: Memoirs Geological Society. https://doi.org/10.1144/M43.

Chardon, D., Jayananda, M., Chetty, T. R. K., & Peucat, J. J. (2008). Precambrian continental strain and shear zone patterns: The South Indian case. *Journal of Geophysical Research*, *113*, B08402. https://doi.org/10.1029/2007JB005299.

Chatterjee A. (2017). *Geochemistry of magmatic rocks in the Kadiri greenstone belt: implications on crustal growth and mineralization in EDC* (Unpublished PhD thesis; 241 p.). Osmania University.

Chatterjee, A., Lingamurty, E., Singh, R., & Manikymba, C. (2013). Geochemical signatures of volcanic rocks from Kadiri greenstone belt, Dharwar Craton, India: Implications on Gold mineralization. *Mineralogical Magazine*, *77*, 805–933. https://doi.org/10.1180/minmag.2013.077.5.3.

Dey, S. (2013). Evolution of Archaean crust in the Dharwar craton: the Nd isotope record. *Precambrian Research*, *227*, 227–246.

Dey, S., Nandy, J., Choudhary, A. K., Liu, Y., & Zong, K. (2014). Origin and evolution of granitoids associated with the Kadiri greenstone belt, eastern Dharwar craton: a history of orogenic to anorogenic magmatism. *Precambrian Research*, *246*, 64–90.

Dey, S., Nandy, J., Choudhary, A.K., Liu, Y., & Zong, K. (2015). Neoarchaean crustal growth by combined arc-plume action: evidence from the Kadiri Greenstone Belt, Eastern Dharwar craton, India. Geological Society of London, Special Publications, 389, 135–163.

Drury, S. A., Harris, N. B. W., Holt, R. W., Reeves-Smith, G. J., & Wightman, R. T. (1984). Precambrian tectonics and crustal evolution in South India. *The Journal of Geology*, *92*, 3–20.

Fischer, R. V., & Schmincke, H. U. (1984). *Alteration of volcanic glasses* (pp. 312–345). Berlin: Pyroclastic Rocks. Springer-Verla g.

Ganguly, S., Manikyamba, C., Saha, A., Lingadevaru, M., Santosh, M., Rambabu, S., … Linga, D. (2016). Geochemical characteristics of gold bearing boninites and banded iron formations from Shimoga greenstone belt, India: Implications for gold genesis and hydrothermal processes in diverse tectonic settings. *Ore Geology Reviews*, *73*, 59–82.

Ganguly, S., & Yang, Q. Y. (2018). Greenstone belts and their mineral endowment: Preface. *Geoscience Frontiers*, *9*, 599–601.

Ghose, N. C. (2019). *Pyroclastic Rocks of India: In space and time*. Roorkee: Indian Geological Congress.

Giritharan, T. S., & Rajamani, V. (1998). Geochemistry of the metavolcanics of the Hutti-Maski schist belt, South India: implications to gold metallogeny in the eastern Dharwar Craton. *Journal of the Geological Society of India*, *51*, 583–594.

Gupta, S., Rai, S. S., Prakasam, K. S., Srinagesh, D., Bansal, B. K., Chadha, R. K., … Gaur, V. K. (2003). The nature of the crust in southern India: implicationsfor Precambrian crustal evolution. *Geophysical Research Letters*, *30*, 1419.

Hawkesworth, C. J., & Kemp, A. I. S. (2006). Evolution of the continental crust. *Nature*, *443*, 811–817.

Hokada, T., Horie, K., Satish-Kumar, M., Ueno, Y., Nasheeth, A., Mishima, K., & Shiraishi, K. (2013). An appraisal of Archaean supracrustal sequences in Chitradurga Schist Belt, Western Dharwar Craton, Southern India. *Precambrian Research*, *227*, 99–119. https://doi.org/10.1016/j.precamres.2012.04.006.

Jayananda, M., Chardon, D., Peucat, J. J., & Capdevila, R. (2006). 2.61 Ga potassic granites and crustal reworking in the western Dharwar Craton, southern India: Tectonic, geochronologic and geochemical constraints. *Precambrian Research*, *150*, 1–26.

Jayananda, M., Moyen, J. F., Martin, H., Peucat, J. J., Aurvay, B., & Mahabaleswar, B. (2000). Late Archaean (2550-2520) juvenile magmatism in the eastern Dharwar Craton, southern India: Constraints from geochronology, Nd-Sr isotopes and whole rock geochemistry. *Precambrian Research*, *99*, 225–254.

Jayananda, M., Peucat, J.-J., Chardon, D., Krishnarao, B., & Corfu, F. (2013). Neoarchean greenstone volcanism, Dharwar Craton, southern India: Constraints from SIMS zircon geochronology and Nd isotopes.

*Precambrian Research*, *227*, 55–76. https://doi.org/10.1016/j.precamres.2012.05.002.

Kazmi, S. M. K., & Kumar, C. G. (1991). *Regional geochemical surveys in Kadiri schist belt, Anantapur and Chitoor districts, A.P. Records of Geological survey of India 124* (pp. 30–31).

Manikyamba, C., Ganguly, S., Saha, A., Santosh, M., Rajanikanta Singh, M., & Subba Rao, D. V. (2014). Continental lithospheric evolution: Constraints from the geochemistry of felsic volcanic rocks in the Dharwar Craton, India. *Journal of Asian Earth Sciences*, *95*, 65–80. https://doi.org/10.1016/j.jseaes.2014.05.015.

Manikyamba, C., Ganguly, S., Santosh, M., Singh, M. R., & Saha, A. (2015). Arc-nascent back-arc signature in meta basalts from the Neoarchean Jonnagiri greenstone terrane, eastern Dharwar Craton. *Indian Geology Journal*, *50*, 651–669.

Manikyamba, C., Ganguly, S., Santosh, M., & Subramanyam, K. S. V. (2017). Volcano-sedimentary and metallogenic records of the Dharwar greenstone terranes, India: Window to Archean plate tectonics, continent growth, and mineral endowment. *Gondwana Research*, *50*, 38–66.

Manikyamba, C., Kerrich, R., Naqvi, S. M., & Ram Mohan, M. (2004). Geochemical systematics of tholeiitic basalts from the 2.7Ga Ramagiri-Hungund composite greenstone belt, Dharwar Craton. *Precambrian Research*, *134*, 21–39.

Manikyamba, C., Naqvi, S. M., Mohan, M. R., & Rao, T. G. (2004). Gold mineralisation and alteration of Penakacherla schist belt, India, constraints on Archaean subduction and fluid processes. *Ore Geology Reviews*, *24*, 199–227.

Manikyamba, C., & Saha, A. (2014). PGE Geochemistry of Komatiites from Neoarchean Sigegudda Greenstone Terrane, Western Dharwar Craton, India. *Geological Society of India, Special Publication* (Vol. *2*, pp. 162–174).

Manikyamba, C., Saha, A., Santosh, M., Ganguly, S., Singh, R., Subba Rao, D. S., & Lingadevaru, M. (2014). Neoarchaean felsic volcanic rocks from the Shimoga greenstone belt, Dharwar Craton, India: Geochemical fingerprints of crustal growth at an active continental margin. *Precambrian Research*, *252*, 1–21. https://doi.org/10.1016/j.precamres.2014.06.014.

Manikyamba, C., Pahari, A., Dhanakumar, T., Chatterjee, A., & Ganguly, S. (2020). Evolution of geodynamic processes in Neoarchen Kadiri greenstone belt, eastern Dharwar Craton, India: implications on the migrating arc magmatism. *Journal of Geodynamics*, *136*, 101717.

Mishra, B., Pruseth, K. L., Hazarika, P., & Chinnasamy, S. S. (2018). Nature and source of the ore-forming fluids associated with orogenic gold deposits in the Dharwar Craton. *Geoscience Frontiers*, *9*, 715–726.

Mukhopadhyay, D. (1986). Structural pattern in the Dharwar Craton. *Journal of Geology*, *94*, 167–186.

Naha, K., Mukhopadhyay, D., Dastidar, S., & Mukhopadhyay, R. P. (1995). Basement-cover relations between a granite gneiss body and its metasedimentary envelope: A structural study from the Early Precambrian Dharwar tectonic province, southern India. *Precambrian Research* (Vol. *72*, 3-4, pp. 283–299).

Naqvi, S. M. (2005). *Geological evolution of the Indian Plate (from Hadean to Holocene- 4Ga to 4Ka)* (p. 450). New Delhi, India: Capital Publication.

Naqvi, S. M., & Rogers, J. J. W. (1987). *Precambrian Geology of India*, Oxford University Press, (p. 1–223). Oxford, England.

Nasheeth, A., Okudaira, T., Horie, K., Hokada, T., & Satish-Kumar, M. (2015). SHRIMP U-Pb zircon ages of granitoids adjacent to Chitradurga shear zone, Dharwar Craton, South India and its tectonic implications. *Journal of Mineralogy and Petrology*, *110*, 224–234.

Nutman, A. P., Chadwick, B., Krishna Rao, B., & Vasudev, V. N. (1996). SHRIMP U/Pb Zircon ages of acid volcanic rocks in the Chitradurga and Sandur Groups, and granites adjacent to the Sandur Schist Belt, Karnataka. *Journal of Geological Society of India*, *47*, 153–164.

Oelkers, E. H., & Poitrasson, F. (2002). An experimental study of the dissolution stoichiometry and rates of a natural monazite as a function of temperature from 50 to 230 C and pH from 1.5 to 10. *Chemical Geology*, *191*, 73–87.

Pal, N., & Mishra, B. (2002). Alteration geochemistry and fluid inclusion characteristics of the greenstone-hosted gold deposit of Hutti, Eastern Dharwar Craton, India. *Mineralium Deposita*, *37*, 722–736.

Pahari, A., Tang, L., Manikyamba, C., Santosh, M., Subramanyam, K. S. V., & Ganguly, S. (2019). Meso-Neoarchean magmatism and episodic crustal growth in the Kudremukh-Agumbe granite-greenstone belt, western Dharwar Craton, India. *Precambrian Research*, *323*, 16–54.

Pearce, J. A. (1996). A user's guide to basalt discrimination diagrams. In (Ed.), *Trace element geochemistry of volcanic rocks: Applications for massive sulphide exploration*, Geological Association of Canada, Short Course Notes, *12*, 79–113.

Peucat, J. J., Mahabaleshwar, B., & Jayananda, M. (1993). Age of younger tonalitic magmatism and granulitic metamorphism in the South India transition zone (Krishnagiri area): Comparison with older Peninsular gneisses from the Gorur Hassan area. *Journal Metamorphic Geology*, *11*, 879–888.

Pichler, H., Schmitt-Riegraf, C., & Hoke, L. (1997). *Rock-forming minerals in thin section* (p. 220). London, England: Chapman & Hall.

Poitrasson, F. (2002). In situ investigations of allanite hydrothermal alteration: Examples from calc-alkaline and anorogenic granites of Corsica (southeast France). *Contributions to Mineralogy and Petrology*, *142*, 485–500.

Price, J. R., Velbel, M. A., & Patino, L. C. (2005). Rates and time scales of clay-mineral formation by weathering in saprolitic regoliths of the southern Appalachians from geochemical mass balance. *Geological Society of America Bulletin*, *117*, 783–794.

Price, R. C., Maillet, P., McDougall, I., & Dupont, J. (1991). The geochemistry of basalts from the Wallis Islands, Northern Melanesian Borderland: Evidence for a lithospheric origin for Samoan-type basaltic magmas? *Journal of Volcanology and Geothermal Research*, *45*, 267–288.

Radhakrishna, B. P. (1983). Archean granite-greenstone terrane of the South Indian shield. *Memoir Geological Society of India*, *4*, 1–46.

Rajamani, V., Shivkumar, K., Hanson, G. N., & Shrey, S. B. (1985). Geochemistry and petrogenesis of amphibolites, Kolar schist belt, South India: evidence for komatiitic magma derived by low percentage of melting of the mantle. *Journal of Petrology*, *26*, 92–123.

Ramakrishnan, M., & Vaidyanadhan, R. (2008). *Geology of India* (p. 556). Bangalore, India: Geological Society of India.

Ramam, P. K., & Murthy, V. N. (1997). *Geology of Andhra Pradesh* (p. 245). Bangalore, India: Geological Society of India.

Reddy, B. V., & Jagadish, K. S. (1993). The static compaction of soils. *Geotechnique*, *43*(2), 337–341.

Roberts, N. M. (2012). Increased loss of continental crust during supercontinent amalgamation. *Gondwana Research*, *21*, 994–1000.

Santosh, M. (2010). A synopsis of recent conceptual models on supercontinent tectonics in relation to mantle dynamics, life evolution and surface environment. *Journal of Geodynamics*, *50*, 116–133.

Santosh, M., Arai, T., & Maruyama, S. (2017). Hadean Earth and primordial continents: The cradle of prebiotic life. *Geoscience Frontiers*, *8*, 309–327.

Sarangi, S., Srinivasan, R., & Balaram, V. (2013). REE geochemistry of auriferous quartz carbonate veins of Neoarchean Ajjanahalli gold deposit, Chitradurga schist belt, Dharwar Craton, India. *Geoscience Frontiers*, *4*, 231–239.

Saravanan, C. S., Mishra, B., & Jairam, M. S. (2009). P–T conditions of mineralization in the Jonnagiri granitoid-hosted gold deposit, eastern Dharwar Craton, southern India: Constraints from fluid inclusions and chlorite thermometry. *Ore Geology Reviews*, *36*, 333–349.

Sarma, D. S., Mcnaughton, N. J., Fletcher, I. R., Groves, D. I., Mohan, M. R., & Balaram, V. (2008). Timing of gold mineralization in the Hutti gold deposit, Dharwar Craton, South India. *Economic Geology*, *103*(8), 1715–1727.

Shaji, E., Santosh, M., He, X. F., Fan, H. R., Dev, S. D., Yang, K. F., … Pradeepkumar, A. P. (2014). Convergent margin processes during Archean–Proterozoic transition in southern India: Geochemistry and zircon U–Pb geochronology of gold-bearing amphibolites, associated metagabbros, and TTG gneisses from Nilambur. *Precambrian Research*, *250*, 68–96.

Sreenivasulu, P., Padmasree, P., & Lakshmidevamma, B. (2013). Mineral potentialities Kadiri Schist belt, Eastern Dharwar Craton, South India – An overview. *International Journal of Basic and Applied Chemical Sciences*, *3*(4), 96–101.

Swain, S. K., Sarangi, S., Srinivasan, R., Sarkar, A., Kesarwani, M., Mazumdar, A., & Satyanarayanan, M. (2018). Stable isotope (COS) and geochemical studies of auriferous quartz carbonate veins, Neoarchaean orogenic Ajjanahalli and Gadag Gold Field, Chitradurga schist belt, Dharwar Craton, southern India: Implication for the source of gold mineralizing fluids. *Ore Geology Reviews*, *95*, 456–479.

Swami Nath, J., Ramakrishnan, M., & Viswanatha, M. N. (1976). Dharwar stratigraphic model and Karnataka craton evolution. *Geological Survey of India Record*, *107*, 149–175.

Taunton, A. E., Welch, S. A., & Banfield, J. F. (2000). Geomicrobiological controls on light rare earth element, Y and Ba distributions during granite weathering and soil formation. *Journal of Alloys and Compounds*, *303*, 30–36.

Zachariah, J. K., Mohanta, M. K., & Rajamani, V. (1996). Accretionary evolution of the Ramagiri schist belt, Eastern Dharwar Craton. *Journal of Geological Society of India*, *47*, 279–291.

## SUPPORTING INFORMATION

Additional supporting information may be found online in the Supporting Information section at the end of this article.

**How to cite this article:** Manikyamba C, Ghose NC, Ganguly S, Pahari A, Sindhuja CS. Gold, uranium, thorium, and rare earth mineralization in the Kadiri Volcanic Province of Eastern Dharwar Craton, India: An evaluation of mineralogical, textural, and geochemical attributes. *Geological Journal*. 2020; 1–23. https://doi.org/10.1002/gj.3959